TABLE IV. Organ weights of male and female rats administered PFDoA

		Main Group				Recovery Group	
Dose (mg/kg/day)		0 (control)	0.1	0.5	2.5	0 (control)	2.5
MALES							
Number of animals examined		5	5	5	5	5	5
Liver	(g)	12.0 ± 1.3	13.5 ±2.1	14.7 ±2.6	13.6 ±3.1	13.1 ± 1.2	15.2 ±2.8
	(%)[a]	2.51 ±0.14	2.67 ±0.21	3.00 ± 0.30*	4.30 ±0.27**	2.56 ±0.18	3.94 ±0.61**
Kidney[b]	(g)	3.01 ±0.27	3.28 ±0.22	3.26 ± 0.43	2.39 ±0.45*	3.15 ±0.14	2.76 ±0.21**
	(%)[a]	0.628 ±0.032	0.656 ±0.052	0.670 ± 0.058	0.760 ± 0.060**	0.614 ±0.029	0.718 ± 0.050**
Spleen	(g)	0.784 ±0.102	0.802 ±0.091	0.724 ± 0.123	0.488 ±0.155**	0.862 ±0.074	0.650 ± 0.025**
	(%)[a]	0.166 ±0.015	0.158 ±0.015	0.148 ± 0.013	0.152 ±0.029	0.170 ±0.019	0.170 ±0.010
Heart	(g)	1.480 ±0.180	1.520 ±0.150	1.390 ± 0.160	0.864 ±0.180**	1.480 ±0.094	1.110 ±0.110**
	(%)[a]	0.312 ±0.041	0.300 ±0.016	0.288 ± 0.029	0.274 ±0.013	0.292 ±0.023	0.286 ±0.011
Brain	(g)	2.21 ±0.13	2.14 ±0.10	2.16 ± 0.03	2.10 ±0.12	2.21 ±0.01	2.15 ±0.08
	(%)[a]	0.460 ±0.020	0.428 ±0.033	0.446 ± 0.034	0.688 ±0.160**	0.430 ±0.032	0.562 ±0.049**
Pituitary gland	(mg)	12.3 ±0.8	12.3 ±0.6	13.0 ±2.1	7.5 ± 1.6**	12.2 ±2.2	9.4 ± 1.5*
	(10^{-3}%)[a]	2.57 ±0.05	2.46 ±0.27	2.68 ± 0.51	2.37 ±0.30	2.40 ±0.43	2.44 ±0.33
Thymus	(mg)	325 ±97	442 ±75	328 ± 86	133 ±79**	382 ± 114	239 ±62*
	(10^{-3}%)[a]	67.6 ± 19.9	87.8 ± 12.7	67.0 ± 15.3	39.1 ± 18.9*	75.3 ±24.2	62.5 ± 19.0
Thyroid	(mg)	23.3 ±3.7	23.7 ± 1.5	22.3 ± 4.3	14.4 ±4.1**	22.4 ±3.7	16.2 ±3.8*
	(10^{-3}%)[a]	4.87 ±0.81	4.73 ±0.30	4.61 ± 1.00	4.53 ±0.77	4.38 ±0.61	4.22 ±0.96
Adrenal gland	(mg)	65.0 ±8.5	68.4 ±9.8	63.4 ± 17.0	38.4 ±5.9**	62.4 ±8.6	40.4 ±6.2**
	(10^{-3}%)[a]	13.5 ± 1.3	13.6 ± 1.9	13.2 ±3.9	12.5 ±2.9	12.3 ± 1.9	10.5 ± 1.5
Testis[b,c]	(g)	3.36 ±0.37	3.34 ±0.23	3.39 ± 0.30	2.81 ±0.65	3.43 ±0.28	3.39 ±0.42
	(%)[a]	0.671 ±0.054	0.647 ±0.049	0.677 ± 0.080	0.839 ±0.160	0.672 ±0.077	0.882 ±0.110**
Epididymis[b,c]	(g)	1.33 ±0.17	1.35 ±0.12	1.32 ± 0.10	0.90 ±0.31**	1.43 ±0.090	1.23 ±0.13*
	(%)[a]	0.267 ±0.033	0.263 ±0.024	0.263 ± 0.020	0.266 ±0.073	0.280 ±0.025	0.316 ±0.017*
FEMALES							
Number of animals examined		5	5	5	1	5	5
Liver	(g)	9.9 ±0.6	10.8 ±0.9	10.9 ± 0.9	10.9[d]	7.6 ±0.4	8.7 ± 1.8
	(%)[a]	3.23 ±0.19	3.43 ±0.11	3.70 ± 0.22**	4.52[d]	2.45 ±0.11	3.61 ±0.35**
Kidney[b]	(g)	2.19 ±0.17	2.06 ±0.22	1.97 ± 0.09	1.86[d]	2.02 ±0.08	1.99 ±0.29
	(%)[a]	0.720 ±0.093	0.656 ±0.038	0.668 ± 0.022	0.780[d]	0.656 ±0.022	0.836 ± 0.063**
Spleen	(g)	0.780 ±0.052	0.750 ±0.046	0.674 ± 0.081*	0.400[d]	0.560 ±0.100	0.522 ±0.110
	(%)[a]	0.256 ±0.040	0.240 ±0.019	0.232 ± 0.023	0.170[d]	0.182 ±0.035	0.218 ±0.035
Heart	(g)	1.040 ±0.090	1.080 ±0.054	0.928 ± 0.048*	0.770[d]	0.994 ±0.036	0.796 ±0.160*
	(%)[a]	0.342 ±0.022	0.346 ±0.018	0.316 ± 0.017	0.320[d]	0.324 ±0.011	0.334 ±0.034
Brain	(g)	2.02 ±0.11	2.00 ±0.06	2.00 ± 0.02	2.14[d]	2.10 ±0.09	1.99 ±0.09
	(%)[a]	0.662 ±0.057	0.640 ±0.041	0.680 ± 0.025	0.890[d]	0.682 ±0.028	0.852 ±0.150*
Pituitary gland	(mg)	17.3 ± 1.7	16.0 ±2.3	14.1 ± 1.9*	12.0[d]	17.7 ±2.2	10.4 ±4.5*
	(10^{-3}%)[a]	5.67 ±0.71	5.13 ±0.87	4.80 ± 0.60	5.00[d]	5.75 ±0.75	4.27 ± 1.3
Thymus	(mg)	310 ±27	297 ± 102	264 ± 16**	66.0[d]	298 ±70	241 ± 137
	(10^{-3}%)[a]	101.0 ± 11.2	93.7 ±27.8	89.5 ±3.8	27.5[d]	96.9 ±23.9	95.9 ±50.3
Thyroid	(mg)	17.8 ±4.7	18.8 ±3.7	18.3 ±4.2	11.0[d]	15.5 ± 1.5	13.1 ±5.6
	(10^{-3}%)[a]	5.74 ± 1.10	6.01 ± 1.20	6.21 ± 1.30	4.58[d]	5.02 ±0.47	5.32 ± 1.70
Adrenal gland	(mg)	84.2 ± 13.0	77.2 ± 8.6	79.4 ± 5.0	53.0[d]	70.8 ±9.2	47.4 ± 12.0**
	(10^{-3}%)[a]	27.5 ± 4.3	24.7 ± 3.3	27.0 ± 1.5	22.1[d]	23.0 ±3.1	19.9 ± 3.3
Ovary[b]	(mg)	115.4 ± 14.3	114.0 ± 21.1	109.6 ± 10.0	119.0[d]	100.4 ±17.4	56.0 ± 7.3**
	(10^{-3}%)[a]	37.6 ± 3.3	36.2 ± 4.7	37.2 ± 3.1	49.6[d]	32.6 ±6.0	23.7 ± 3.1*

Values are given as the mean ± S.D.

*Significantly different from the control, at $p \leq 0.05$.

**Significantly different from the control, at $p \leq 0.01$.

[a]Ratio of absolute organ weight to body weight on the necropsy day (relative organ weight).

[b]Values are represented as the total weights of the organs on both sides.

[c]Organ weight was measured for all animals (number of examined animals: 7 at 0 and 2.5 mg/kg/day and 12 at 0.1 and 0.5 mg/kg/day in the main group, and 5 at 0 and 2.5 mg/kg/day in the recovery group).

[d]Data from only one animal. In this group, other females did not deliver pups normally or survive to the end of the study.

TABLE V. Histopathological findings in male and female rats administered PFDoA

		Main Group				Recovery Group	
Dose (mg/kg/day)	Grade	0 (control)	0.1	0.5	2.5	0 (control)	2.5
MALES							
Number of animals examined		7	12	12	7	5	5
Forestomach							
Erosion	+	0	0	0	1	0	0
Hyperkeratosis	+	0	0	0	2	0	0
Hyperplasia in squamous cells	+	0	0	0	2	0	0
Infiltration of inflammatory cells in the submucosa	+	0	0	0	1	0	0
Fibrosis of the submucosa	+	0	0	0	2	0	0
Pancreas							
Decrease in zymogen granules	+	0	0	0	5]**	0	1
	++	0	0	0	1]	0	0
Liver							
Deposition of bilirubin	+	0	0	0	1	0	2
Peribiliary infiltration of inflammatory cells	+	0	0	0	4	0	4*
Single cell necrosis of hepatocytes	+	0	0	0	1	0	0
	++	0	0	0	1	0	0
Focal necrosis	+	0	0	0	3	0	0
	++	0	0	0	1	?0	0
Diffuse hepatocyte hypertrophy	+	0	0	0	5*	0	3
Centrolobular hepatocyte hypertrophy	+	0	0	0	0	0	2
Periportal fatty changes	+	0	0	0	1	0	0
Fatty changes in midzonal	+	0	0	0	1	0	0
Fatty changes in diffuse	+	0	0	0	1	0	0
Testis							
Cell debris (Stage VII–VIII)	+	0	0	0	1	0	0
Decrease in elongated spermatids (Stage XII–XIV)	+	0	0	0	2	0	0
Epididymis							
Decrease in spermatozoa	+	0	0	0	2	0	1
	++	0	0	0	1	0	0
	+++	0	0	0	1	0	0
Cell debris in the lumen	+	0	0	0	2	0	0
	++	0	0	0	1	0	0
Spermatic granuloma	+	0	0	0	2	0	0
Prostate							
Glandular epithelium atrophy	+	0	0	0	3	0	1
Fibrosis in the interstitium	+	0	0	0	1	0	0
Seminal vesicles							
Glandular epithelium atrophy	+	0	0	0	3	0	1
	++	0	0	0	1	0	0
Coagulating gland							
Glandular epithelium atrophy	+	0	0	0	3	0	1
	++	0	0	0	1	0	0
Spleen							
White pulp atrophy	+	0	0	0	1	0	0
Red pulp atrophy	+	0	0	0	3	0	0
Thymus							
Atrophy of the cortex	+	0	0	0	0	0	1
	++	0	0	0	1	0	0
	+++	0	0	0	2	0	0
Bone marrow							
Decrease in hematopoiesis	+	0	0	0	2	0	0
	++	0	0	0	2	0	0
Adrenal glands							

TABLE V. *Continued*

		Main Group				Recovery Group	
Dose (mg/kg/day)	Grade	0 (control)	0.1	0.5	2.5	0 (control)	2.5
Atrophy of the cortex	+	0	0	0	5*	0	0
Skeletal muscle							
Muscle fiber atrophy	+	–	–	–	2(3)	–	–
	++	–	–	–	1(3)	–	–
FEMALES							
Number of animals examined		12	12	12	12[a]	5	5
Forestomach							
Edema of the submucosa	+	0	0	0	1	0	0
Glandular stomach							
Ulcer	+	0	0	0	4	0	0
Pancreas							
Edema of the interstitium	+	0	0	0	5 *	0	0
	++	0	0	0	1	0	0
Decrease in zymogen granuled	+	0	0	0	2	0	2
	++	0	1	0	1	0	0
Liver							
Deposition of bilirubin	+	0	0	0	1	0	5**
Single cell necrosis of hepatocytes	+	0	0	0	2 *	0	3
	++	0	0	0	5	0	0
Focal necrosis	+	0	0	2	4	0	0
Centrilobular hepatocyte necrosis	++	0	0	0	1	0	0
Bile duct proliferation	+	0	0	0	1	0	2
	++	0	0	0	1	0	2 **
Diffuse hepatocyte hypertrophy	+	0	0	0	6 **	0	2
	++	0	0	0	6	0	3
Inflammatory cell infiltration in peribiliary	+	0	0	0	0	0	3
Increase in mitosis in hepatocytes	+	0	0	0	1	0	0
Fatty changes in periportal	+	1	0	0	0	0	0
Fatty changes in diffuse	++	0	0	0	0	0	1
Uterus							
Hemorrhage at the implantation site	+	0	0	0	7 **	0	0
	++	0	0	0	1	0	0
Congestion of the endometrium	+	0	0	0	4	0	0
	++	0	0	0	1	0	0
Atrophy of endometrium and myometrium	+	0	0	0	0	0	2
Spleen							
White pulp atrophy	+	0	0	0	1(9)	0	1
	++	0	0	0	2 (9)	0	0
Red pulp atrophy	+	0	0	0	2(9)	0	0
	++	0	0	0	1(9)	0	0
Thymus							
Atrophy of the cortex	+	0	0	0	3 (10) **	0	1
	++	0	0	0	4 (10)	0	0
	+++	0	0	0	2 (10)	0	0
Bone marrow							
Decrease in hematopoiesis	+	0	0	0	2 (10)	0	1
Adrenal glands							
Atrophy of the cortex	+	0	0	0	0	0	5**
Skeletal muscle							
Muscle fiber atrophy	+	–	–	–	–	–	1(1)

Values are the number of animals with findings.
Values in parentheses are the number of animals examined.
–, Not examined; Grade +, slight change; ++, moderate change; +++, severe change.
[a]Including animals euthanized and found dead.
*Significantly different from the control, at $p \leq 0.05$.
**Significantly different from the control, at $p \leq 0.01$.

TABLE VI. Reproductive performance and developmental findings in rats administered PFDoA

Dose (mg/kg/day)			0 (control)	0.1	0.5	2.5
MAIN GROUP						
Premating period						
Estrous cycle normality			12/12	12/12	11/12	12/12
Length (days)[a]			4.13 ±0.30	4.29 ±0.54	4.18 ±0.43	4.23 ±0.41
Number of pairs			12	12	12	12
Copulation index (%)		Male	100	100	100	100
		Female	100	100	100	100
Fertility index (%)			100	91.7	100	100
Gestation index (%)			100	100	100	8.33**
Gestation length (days)[a]			22.1 ±0.3	22.2 ±0.4	22.1 ±0.3	23.0[b]
Number of pregnant animals			12	11	12	12
Number of corpora lutea[a]			17.1 ± 1.6	16.9 ± 1.3	15.8 ± 1.5	15.4 ±2.2
Number of implantation sites[a]			16.0 ± 1.3	16.6 ± 1.3	15.5 ± 1.4	14.5 ±2.1
Implantation index (%)[a]			93.9 ±4.8	98.4 ±2.7[d]	98.5 ±3.7[d]	94.4 ±8.9
Delivery index (%)[a]			94.3 ±6.3	91.7 ±6.5	89.7 ±9.7	31.4 ±54.0[c]
Number of litters			12	11	12	1
Number of pups delivered[a]		Total	15.1 ± 1.5	15.3 ± 1.7	13.9 ±2.0	16.0[b]
		Alive	15.1 ± 1.5	14.9 ± 1.8	13.8 ±2.1	14.0[b]
		Dead	0.0 ±0.0	0.4 ±0.7	0.1 ±0.3	2.0[b]
Sex ratio of live pups[a]			0.55 ±0.10	0.61 ±0.10	0.57 ±0.13	0.43[b]
Live birth index (%)[a]			100.0 ±0.0	97.6 ±4.6	99.3 ±2.4	87.5[b]
Number of live pups[a]	on nursing day 4		14.8 ± 1.3	14.6 ± 1.7	13.6 ±2.0	14.0[b]
Viability index (%)[a]			98.5 ±2.8	98.3 ±3.0	98.3 ±3.0	100[b]
Male pups						
Body weight (g)[a]	PND 0		6.48 ±0.30	6.52 ±0.64	6.70 ±0.52	4.70[b]
	PND 1		7.08 ±0.33	7.12 ±0.79	7.33 ±0.71	4.90[b]
	PND 4		10.50 ±0.63	10.70 ± 1.20	10.70 ± 1.40	6.20[b]
Female pups						
Body weight (g)[a]	PND 0		6.19 ±0.28	6.17 ±0.51	6.26 ±0.65	4.70[b]
	PND 1		6.81 ±0.32	6.75 ±0.62	7.01 ±0.68	5.00[b]
	PND 4		10.10 ±0.50	10.00 ± 1.10	10.20 ± 1.40	6.50[b]
RECOVERY GROUP						
Administration period						
Estrous cycle normality			5/5			0/5[e]
Length (days)[a]			4.24 ±0.43			-[d]
Recovery period						
Estrous cycle normality			5/5			1/5*
Length (days)[a]			4.10 ±0.22			4.00[e]

Estrous cycle normality, number of females with a normal estrous cycle / number of females examined; Copulation index, (number of animals with successful copulation / number of animals mated) × 100; Fertility index, (number of pregnant females/number of pairs with successful copulation) × 100; Gestation index, (number of females with live pups/number of pregnant females) × 100; Implantation index, (number of implantation sites/number of corpora lutea) × 100; Delivery index, (number of pups born/number of implantation sites) × 100; Sex ratio, (number of live male pups/number of live pups); Live birth index, (number of live pups on nursing day 0/number of pups born) × 100; Viability index, (number of live pups on nursing day 4/number of live pups on nursing day 0) × 100.

[a]Values are means and S.D.

[b]The number of dams or litters examined was one because only one dam normally delivered pups. The data were excluded from statistical evaluation.

[c]The number of litters examined was three because seven animals were found dead or moribund at the end of pregnancy and two females did not deliver pups normally. The data were excluded from statistical evaluation.

[d]Since continuous diestrous was observed in all five females, the length of the estrous cycle could not be calculated.

[e]The length of the estrous cycle was only calculated for one female because continuous diestrous was observed in the four other females. The data were excluded from statistical evaluation.

*Significantly different from the control, at $p \leq 0.05$.

**Significantly different from the control, at $p \leq 0.01$.

stages VII–VIII and a decrease in the number of elongate spermatids at stages XII–XIV in the testis, decrease in spermatozoa, cell debris in the lumen and spermatic granuloma in the epididymis, and fibrosis of the interstitium in the prostate were found. In female reproductive organs, hemorrhage on the implantation site and/or congestion on the endometrium were detected in the uterus of all 7 females found dead or moribund at the end of the gestation period. Hemorrhage at the implantation site was also found in one female that did not deliver live pups (all pups were stillborn).

Most hepatic changes remained after the 14-day recovery period (Table V). The incidences of peribiliary inflammatory cellular infiltration in males and bilirubin deposition and diffuse hepatocyte hypertrophy in females were significantly higher in the 2.5 mg/kg/day recovery group. Atrophy of the adrenal cortex was observed in all females in the 2.5 mg/kg/day recovery group with a significantly higher incidence. Endometrium and myometrium atrophy was noted in the uterus in 2 of 5 females given 2.5 mg PFDoA/kg/day after the 14-day recovery period. Although histopathological changes were also observed in the pancreas, thymus, spleen, bone marrow, skeletal fibers, and male reproductive organs after the 14-day recovery period, their incidences or degree was generally lower than those at the end of the administration period.

Reproductive and Developmental Findings

All females in the main group exhibited a normal estrous cycles during the premating period, except for one female in the 0.5 mg/kg/day group in which persistent diestrous was noted (Table VI). No significant deviations were observed in the incidence of a normal estrous cycle and length of the estrous cycle during the premating period. On the other hand, continuous diestrous was observed in the recovery group from day 27 of the administration period in all females given 2.5 mg/kg/day. A normal estrous cycle could not be recovered in four of the five females, even after termination of the administration period.

All males and females in the main groups were successfully copulated (Table VI). Although one female was not impregnated in the 0.1 mg/kg/day group, all other females became pregnant. No significant changes were found in the fertility index, the number of corpora lutea, or the number of implantation sites between the control and PFDoA-treated groups. In the 2.5 mg/kg/day group, 7 of 12 females given 2.5 mg PFDoA/kg/day were found dead or fell into a moribund state at the end of pregnancy, as mentioned above. Two of five surviving pregnant females did not deliver any pups, and 2 other females did not deliver live pups (all pups were stillborn). Consequently, only one female delivered live pups in the 2.5 mg/kg/day group; therefore, the gestation and delivery indices in this group were markedly lower than those of the control group. The gestation length of this one female in the 2.5 mg/kg/day group did not differ from that in the other groups.

The number of normally delivered pups in the 2.5 mg/kg/day group was 16 in one litter; however, two of them were found dead on nursing day 0 (Table VI). Although the other 14 pups survived to the end of the study, their body weights on PNDs 0, 1, and 4 were markedly lower than those of the control group. Necropsy of dead pups revealed renal pelvis dilatation and ascites in one pup in the 0.5 mg/kg/day group, while no other gross external or internal alterations were found in pups that survived until PND 4 or pups found dead during the postnatal period. No significant changes were observed in any reproductive/developmental parameters in the 0.1 and 0.5 mg/kg/day groups.

DISCUSSION

In this study, 7/12 females receiving 2.5 mg PFDoA/kg/day were found dead or moribund at the end of pregnancy. In contrast, no clear dose-related clinical signs of toxicity were observed in females of the recovery group or in males, which suggested that the cause of death involved factors that associated with pregnancy or delivery. Vaginal hemorrhage and/or blood retention in the uterus were observed in the dead and moribund females. Histopathological examinations of the uterus revealed hemorrhage in the implantation sites and congestion of the endometrium. These findings demonstrated that these females could not maintain a pregnancy, and excessive bleeding after placental separation may worsen their general condition.

Food consumption and body weight gain were markedly decreased in both sexes in the 2.5 mg/kg/day group. The effects on body weight are typically observed in rodents given PFCAs at relatively high doses, but they were not accompanied with reduced food intake necessarily (ATSDR, 2009; Hirata-Koizumi et al., 2012). Interestingly, Yang et al. (2002) reported that a 7-day dietary treatment with PFOA lowered the body weight of mice and this effect disappeared when peroxisome proliferator activated receptor (PPAR) α, a nuclear receptor important in regulating fatty acid metabolism in tissues such as liver, kidney, heart, and intestinal mucosa (Corton et al., 2000), was knocked out. PFDoA was recently shown to activate mouse PPARα in transiently transfected COS-1 cells (Wolf et al., 2012). Although no data are currently available on the interaction between PFDoA and rat PPARα, the significant induction of the mRNA levels of important PPARα target genes, acyl CoA oxidase and CYP4A1, was demonstrated in male rats orally dosed with PFDoA at 1 mg/kg and higher for 14 days (Zhang et al., 2008) and at 0.2 mg/kg/day and higher for 110 days (Ding et al., 2009). Taken together, these findings suggest that PFDoA may inhibit body weight gain via the activation of PPARα. In our studies for PFDoA and PFOdA, hepatic necrosis was observed at a dose affecting the body

weight (Hirata-Koizumi et al., 2012); therefore, there is also the possibility that hepatic necrosis is one factor for inhibition of body weight gain.

As with PFOA and the other PFCAs, the primary target of PFDoA was the liver. Relative liver weights increased in both sexes in the 0.5 and 2.5 mg/kg/day groups. Various histopathological changes, including hepatocyte hypertrophy and necrosis, were observed in the liver in both sexes given 2.5 mg PFDoA/kg/day, and focal necrosis was also found in the liver of 2/12 females receiving 0.5 mg PFDoA/kg/day. These changes have been attributed, at least in part, to PPARα activation by PFDoA because PPARα is considered to mediate the biological effects of peroxisome proliferators, such as increases in liver weight due to hepatocyte hypertrophy and hyperplasia, transcriptional increases in enzymes involved in the metabolism of fatty acids, and hepatocarcinogenesis (Green, 1995; Holden et al., 1999; Corton et al., 2000). On the other hand, the following findings suggest that a different mechanism from PPARα activation is involved in the hepatotoxicity of PFDoA. The peribiliary infiltration of inflammatory cells, bilirubin deposition, and proliferation of the bile duct were observed in the 2.5 mg/kg/day group, and blood biochemical examinations revealed an increased level of T-Bil and γ-GTP activity at 2.5 mg/kg/day and increased ALP activity at 0.5 and 2.5 mg/kg/day. These changes indicate inflammatory cholestasis. Yellow brown discoloration of the liver and subcutis, and yellow mass and patch on the epididymis observed in some animals given 2.5 mg PFDoA/kg/day may have resulted from the accumulation of yellow bilirubin pigment. The dose-independent changes in serum T-Cho observed in males suggest that the hypocholesterolemic action of PFDoA via PPARα activation may have been countervailed by impaired cholesterol excretion associated with cholestasis in the high dose group.

Most of the other changes observed in the 2.5 mg/kg/day group may be secondary effects that occur with the pronounced reduction in body weight gain and food consumption. A reduction in motor activity and grip strength may reflect muscle weakness accompanying decreases in body weight rather than neurotoxicity. Atrophy of the lateral great muscle in the 2.5 mg/kg/day group supports this hypothesis. Histopathological changes observed in the stomach, thymus, pancreas, and bone marrow are known to be associated with nutrient deficiencies and/or stress. The prolonged administration of PFDoA, which had a marked influence on food consumption and body weight, must have been stressful for animals. On the other hand, atrophy of the adrenal gland cannot only be explained by changes in body weight and food consumption because previous food restriction studies demonstrated that the adrenal gland was hypertrophied (Moriyama et al., 2008; Shallie et al., 2012). Such atrophic changes in the adrenal gland were shown to be induced by adrenal steroidogenesis inhibitors such as 1-(o-chlorophenyl)−1-(p-chlorophenyl)−2,2-dichloroethane (o,p'-DDD), and α-[1,4-dioxido-3-methylquinoxalin-2-yl]-*N*-methylnitrone (DMNM) (Hamid et al., 1974; Rosol et al., 2001). Because PFDoA was demonstrated to inhibit steroidogenesis in the testis and ovary (Shi et al., 2007; Shi et al., 2009a,b; 2010a,b), it may also alter adrenal steroidogenesis to cause atrophy of the adrenal cortex.

PFDoA affected the male and female reproductive systems. In males, cell debris and a reduction in the number of spermatid or spermatozoa were observed in the testis and epididymis, and atrophic changes were identified in the prostate, seminal vesicle, and coagulating gland in the 2.5 mg/kg/day group. Although these changes may have been due to the inhibition of body weight gain, a previous study demonstrated that the oral administration of PFDoA to rats for 110 days at a dose as low as 0.2 mg/kg/day decreased serum testosterone levels without affecting body weight (Shi et al., 2009a). An *in vitro* study reported the dose-dependent inhibition of steroidogenesis in mouse Leydig tumor cells and primary rat Leydig cells (Shi et al., 2010a), which indicated that PFDoA directly affected testicular testosterone synthesis, and not via the hypothalamic-pituitary-testicular axis. Since decreased testosterone biosynthesis is known to result in the degeneration and reduction in the number of germ cells as well as decreased size of accessory sex glands (O'Connor et al., 2002; OECD, 2009), the histopathological changes observed in the male reproductive organs in this study were attributed, at least in part, to the disruption of steroidogenesis. Shi et al. (2007, 2009a) reported that levels of the steroidogenic acute regulatory protein (StAR), which is responsible for cholesterol transport to the inner mitochondrial membrane, and StAR mRNA were markedly decreased in the testes of rats exposed to PFDoA, and treatment with the hydrosoluble form of cholesterol, which readily enters the inner mitochondrial membrane without the help of StAR, to mouse Leydig tumor cells prevented the inhibitory effect of PFDoA on steroidogenesis (Shi et al., 2010a). These results suggest that StAR is one of the target proteins for PFDoA activity in Leydig cells. A recently conducted proteomic analysis on the testis of rats exposed to PFDoA indicated that alterations in multiple pathways, including mitochondrial disruption and oxidative stress, may be associated with the testicular toxicity of PFDoA in rats (Shi et al., 2010b). Decreased testosterone levels in the testes and/or blood was also caused by PFOA, perfluorononanonic acid (PFNA, C9) and perfluorodecanoic acid (PFDeA, C10) (Bookstaff et al., 1990; Biegel et al., 1995; Jensen et al., 2008; Feng et al., 2009; Feng et al., 2010), which may involve the same mechanism as PFDoA. Recent study on PFOA-induced disruption of testosterone biosynthesis suggests the involvement of PPARα (Li et al., 2011).

A previous study demonstrated that PFDoA decreased serum estradiol levels in female rats following a 28-day oral administration period at a dose that affected body weight (Shi et al., 2009b). Alterations in the ovarian expression of genes responsible for cholesterol transport and steroidogenesis (StAR protein, cholesterol side-chain cleavage enzyme, and 17-beta-hydroxysteroid dehydrogenase) were also found

in this previous study. Such effects on the ovarian steroidogenesis may explain why continuous diestrous was observed in the recovery group in this study because estrogen and progesterone, which are steroid hormones synthesized from cholesterol in the ovary, play an important role in controlling the estrous cycle (OECD, 2009). Continuous diestrous indicates at least the temporary and possibly permanent cessation of follicular development and ovulation, and thus temporary infertility (Parker, 2006). In this study, the lack of an effect on the copulation and fertility indices was consistent with the findings that the abnormal estrous cycle was observed after the 27th day of the administration period in the recovery group and not found during the 14-day premating period in the main group. Considering that continuous diestrous was induced around the same time as changes in body weight and food consumption became apparent, the disruption of energy homeostasis could be a factor in the abnormal estrous cycles observed in this study. Food restriction in rats has been shown to result in weight loss and constant diestrous (Kotsuji et al., 1986; Narita et al., 2011). Recent evidence has suggested that many of the central and peripheral endocrine signals that govern energy homeostasis are involved in the control of reproductive function by acting at different levels of the hypothalamic-pituitary-gonadal axis (Narita et al., 2011). Effects on estrous cyclicity have not been reported for the other PFCAs, which may be because the reproductive toxicity of the other PFCAs were not examined at doses causing severe inhibition of body weight gain as observed in the 2.5 mg/kg/day PFDoA group.

PFDoA exerted no effects on the copulation and fertility indices or on the number of corpora lutea and implantation; however, only one of twelve pregnant females delivered live pups in the 2.5 mg/kg/day group. As mentioned above, PFDoA has been reported to disrupt ovarian steroidogenesis (Shi et al., 2009b). Since pregnancy is maintained under the control of estradiol and progesterone (Ogle et al., 1990; Bartholomeusz et al., 1999), PFDoA may affect pregnancy by disrupting steroidogenesis. Another possible factor is impaired fetal development, which could affect the maintenance of pregnancy and normal delivery. Live pups delivered from one pregnant female in the 2.5 mg/kg/day group had markedly lower body weights than those of the controls. The effects of PFDoA on fetal development could be attributed to secondary effects due to maternal toxicity; however, the lipophilic properties of PFDoA (Inoue et al., 2012) also indicate the possibility that it was transferred via the placenta and directly affected the fetuses.

In this study, some of the changes observed during and at the end of the administration period were detected even after the 14-day recovery period, including reductions in body weight, hypertrophy of hepatocytes, bilirubin disposition, peribiliary infiltration of inflammatory cells and bile duct proliferation in the liver, and atrophy of the adrenal cortex. Although no data are currently available on the toxicokinetics of PFDoA, previous studies demonstrated that PFCAs with a longer carbon chain were eliminated more slowly from the body; the elimination half-life was shown to be 6.38 h for perfluorobutanoic acid (C4), 2.4 h for perfluoroheptanoic acid (C7), 135–185 h for PFOA (C8), 710 hours for PFNA (C9), and 958 h for PFDeA (C10) in male rats intravenously administered PFCAs (Kudo et al., 2002; Kemper, 2003; Ohmori et al., 2003; Chang et al., 2008). Therefore, incomplete recovery of the toxic effects caused by PFDoA may be attributed to its slow elimination from the body.

In summary, 42- to 47-day oral gavage administration of PFDoA mainly affected the liver, causing hypertrophy, necrosis, and inflammatory cholestasis, at 0.5 and 2.5 mg/kg/day. In the 2.5 mg/kg/day group, body weight gain was markedly inhibited, and various changes, mostly viewed as secondary effects, were observed in the bone marrow, spleen, thymus, and adrenal gland. These toxic effects did not recover completely during the 14-day recovery period. Regarding reproductive/developmental toxicity, various histopathological changes, including decreased spermatid and spermatozoa counts, were observed in the male reproductive organs, and continuous diestrous was found in females in the 2.5 mg/kg/day group. Seven of twelve females receiving 2.5 mg/kg/day died during late pregnancy while four other females in this group did not deliver live pups. Based on these findings, the NOAELs of PFDoA were concluded to be 0.1 mg/kg/day for repeated dose toxicity and 0.5 mg/kg/day for the reproductive/developmental toxicity.

REFERENCES

Ahrens L, Siebert U, Ebinghaus R. 2009. Temporal trends of polyfluoroalkyl compounds in harbor seals (Phoca vitulina) from the German Bight, 1999–2008. Chemosphere 76:151–158.

ATSDR. 2009. Toxicological Profile for Perfluoroalkyls (Draft for Public Comment), US Department of health and human services, Public health service, Agency for Toxic Substances and Disease Registry (ATSDR). Accessed on February 28, 2014.

Bartholomeusz RK, Bruce NW, Lynch AM. 1999. Embryo survival, and fetal and placental growth following elevation of maternal estradiol blood concentrations in the rat. Biol Reprod 61:46–50.

Biegel LB, Hurtt ME, Frame SR, O'Connor JC, Cook JC. 2001. Mechanisms of extrahepatic tumor induction by peroxisome proliferators in male CD rats. Toxicol Sci 60:44–55.

Biegel LB, Liu RC, Hurtt ME, Cook JC. 1995. Effects of ammonium perfluorooctanoate on Leydig cell function: in vitro, in vivo, and ex vivo studies. Toxicol Appl Pharmacol 134:18–25.

Bookstaff RC, Moore RW, Ingall GB, Peterson RE. 1990. Androgenic deficiency in male rats treated with perfluorodecanoic acid. Toxicol Appl Pharmacol 104:322–333.

Chang SC, Das K, Ehresman DJ, Ellefson ME, Gorman GS, Hart JA, Noker PE, Tan YM, Lieder PH, Lau C, Olsen GW, Butenhoff JL. 2008. Comparative pharmacokinetics of perfluorobutyrate in rats, mice, monkeys, and humans and relevance to human exposure via drinking water. Toxicol Sci 104:40–53.

Clara M, Scheffknecht C, Scharf S, Weiss S, Gans O. 2008. Emissions of perfluorinated alkylated substances (PFAS) from point sources—Identification of relevant branches. Water Sci Technol 58:59–66.

Corton JC, Lapinskas PJ, Gonzalez FJ. 2000. Central role of PPARalpha in the mechanism of action of hepatocarcinogenic peroxisome proliferators. Mutat Res 448:139–151.

Ding L, Hao F, Shi Z, Wang Y, Zhang H, Tang H, Dai J. 2009. Systems biological responses to chronic perfluorododecanoic acid exposure by integrated metabonomic and transcriptomic studies. J Proteome Res 8:2882–2891.

Falandysz J, Taniyasu S, Gulkowska A, Yamashita N, Schulte-Oehlmann U. 2006. Is fish a major source of fluorinated surfactants and repellents in humans living on the Baltic Coast? Environ Sci Technol 40:748–751.

Feng Y, Fang X, Shi Z, Xu M, Dai J. 2010. Effects of PFNA exposure on expression of junction-associated molecules and secretory function in rat Sertoli cells. Reprod Toxicol 30:429–437.

Feng Y, Shi Z, Fang X, Xu M, Dai J. 2009. Perfluorononanoic acid induces apoptosis involving the Fas death receptor signaling pathway in rat testis. Toxicol Lett 190:224–230.

Fujii Y, Yan J, Harada KH, Hitomi T, Yang H, Wang P, Koizumi A. 2012. Levels and profiles of long-chain perfluorinated carboxylic acids in human breast milk and infant formulas in East Asia. Chemosphere 86:315–321.

Green S. 1995. PPAR: a mediator of peroxisome proliferator action. Mutat Res 333:101–109.

Griffith FD, Long JE. 1980. Animal toxicity studies with ammonium perfluorooctanoate. Am Ind Hyg Assoc J 41:576–583.

Guruge KS, Taniyasu S, Yamashita N, Wijeratna S, Mohotti KM, Seneviratne HR, Kannan K, Yamanaka N, Miyazaki S. 2005. Perfluorinated organic compounds in human blood serum and seminal plasma: A study of urban and rural tea worker populations in Sri Lanka. J Environ Monit 7:371–377.

Hamid J, Sayeed A, McFarlane H. 1974. The effect of 1-(o-chlorophenyl)−1-(p-chlorophenyl)−2,2-dichloroethane(o,p'-DDD) on the immune response in malnutrition. Br J Exp Pathol 55:94–100.

Harada KH, Hitomi T, Niisoe T, Takanaka K, Kamiyama S, Watanabe T, Moon CS, Yang HR, Hung NN, Koizumi A. 2011. Odd-numbered perfluorocarboxylates predominate over perfluorooctanoic acid in serum samples from Japan, Korea and Vietnam. Environ Int 37:1183–1189.

Haug LS, Huber S, Schlabach M, Becher G, Thomsen C. 2011. Investigation on per- and polyfluorinated compounds in paired samples of house dust and indoor air from Norwegian homes. Environ Sci Technol 45:7991–7998.

Haug LS, Thomsen C, Becher G. 2009. Time trends and the influence of age and gender on serum concentrations of perfluorinated compounds in archived human samples. Environ Sci Technol 43:2131–2136.

Hirata-Koizumi M, Fujii S, Furukawa M, Ono A, Hirose A. 2012. Repeated dose and reproductive/developmental toxicity of perfluorooctadecanoic acid in rats. J Toxicol Sci 37:63–79.

Hoff PT, Scheirs J, Van de Vijver K, Van Dongen W, Esmans EL, Blust R, De Coen W. 2004. Biochemical effect evaluation of perfluorooctane sulfonic acid-contaminated wood mice (Apodemus sylvaticus). Environ Health Perspect 112:681–686.

Holden PR, Tugwood JD. 1999. Peroxisome proliferator-activated receptor alpha: Role in rodent liver cancer and species differences. J Mol Endocrinol 22:1–8.

Inoue Y, Hashizume N, Yakata N, Murakami H, Suzuki Y, Kikushima E, Otsuka M. 2012. Unique physicochemical properties of perfluorinated compounds and their bioconcentration in common Carp Cyprinus carpio L. Arch Environ Contam Toxicol 62:672–680.

JALAS. 1987. Guidelines for Animal Experimentation, Japanese Association for Laboratory Animal Science, dated May 22, 1987.

Japanese Animal Welfare Law. 2006. Act on Welfare and Management of Animals. Act No. 105 of October 1, 1973. As amended up to Act No. 50 of June 2, 2006.

Jensen AA, Leffers H. 2008. Emerging endocrine disrupters: Perfluoroalkylated substances. Int J Androl 31:161–169.

Kemper RA. 2003. Perfluorooctanoic acid: Toxicokinetics in the rat. Association of Plastics Manufactures of Europe. Submitted to the US EPA's Admistrative Record. AR226–1499, cited in ASTDR (2009).

Kotsuji F, Goto K, Aso T, Tominaga T. 1986. The influence of weight loss on the reproductive function of the female rat: Changes in the estrous cycle and hypothalamo-pituitary-ovarian function during feed restriction and subsequent refeeding period (in Japanese). Nihon Sanka Fujinka Gakkai Zasshi 38: 1713–1721.

Kudo N, Katakura M, Sato Y, Kawashima Y. 2002. Sex hormone-regulated renal transport of perfluorooctanoic acid. Chem Biol Interact 139:301–316.

Kudo N, Suzuki-Nakajima E, Mitsumoto A, Kawashima Y. 2006. Responses of the liver to perfluorinated fatty acids with different carbon chain length in male and female mice: In relation to induction of hepatomegaly, peroxisomal beta-oxidation and microsomal 1-acylglycerophosphocholine acyltransferase. Biol Pharm Bull 29:1952–1957.

Kunacheva C, Tanaka S, Fujii S, Boontanon SK, Musirat C, Wongwattana T, Shivakoti BR. 2011. Mass flows of perfluorinated compounds (PFCs) in central wastewater treatment plants of industrial zones in Thailand. Chemosphere 83:737–744.

Lau C, Anitole K, Hodes C, Lai D, Pfahles-Hutchens A, Seed J. 2007. Perfluoroalkyl acids: A review of monitoring and toxicological findings. Toxicol Sci 99:366–394.

Li Y, Ramdhan DH, Naito H, Yamagishi N, Ito Y, Hayashi Y, Yanagiba Y, Okamura A, Tamada H, Gonzalez FJ, Nakajima T. 2011. Ammonium perfluorooctanoate may cause testosterone reduction by adversely affecting testis in relation to PPARalpha. Toxicol Lett 205:265–272.

Martin JW, Mabury SA, Solomon KR, Muir DC. 2003. Bioconcentration and tissue distribution of perfluorinated acids in rainbow trout (Oncorhynchus mykiss). Environ Toxicol Chem 22: 196–204.

MOE. 2006. Standards Relating to the Care, Management of Laboratory Animals and Relief of Pain. Announcement No. 88 of Ministry of the Environment (MOE), Japan, dated April 28, 2006.

MOE, METI, MHLW. 2008. Standard concerning testing laboratories implementing tests for new chemical substances etc. Joint notification by director generals of Environmental Policy Bureau, Ministry of the Environment (MOE), Japan (Kanpokihatsu No. 031121004) and Manufacturing Industries Bureau, Ministry of Economy, Trade and Industry (METI), Japan (Seikyokuhatsu No. 3), dated November 17, 2003 and by director general of Pharmaceutical and Food Safety Bureau, Ministry of Health, Labour and Welfare (MHLW), Japan (Yakusyokuhatsu No. 1121003), dated November 21, 2003. As amended up to July 4, 2008.

Moriyama T, Tsujioka S, Ohira T, Nonaka S, Ikeda H, Sugiura H, Tomohiro M, Samura K, Nishikibe M. 2008. Effects of reduced food intake on toxicity study parameters in rats. J Toxicol Sci 33:537–547.

Murakami M, Shinohara H, Takada H. 2009. Evaluation of wastewater and street runoff as sources of perfluorinated surfactants (PFSs). Chemosphere 74:487–493.

Narita K, Nagao K, Bannai M, Ichimaru T, Nakano S, Murata T, Higuchi T, Takahashi M. 2011. Dietary deficiency of essential amino acids rapidly induces cessation of the rat estrous cycle. PLoS One 6:e28136.

Nishikoori H, Murakami M, Sakai H, Oguma K, Takada H, Takizawa S. 2011. Estimation of contribution from non-point sources to perfluorinated surfactants in a river by using boron as a wastewater tracer. Chemosphere 84:1125–1132.

O'Connor JC, Frame SR, Ladics GS. 2002. Evaluation of a 15-day screening assay using intact male rats for identifying steroid biosynthesis inhibitors and thyroid modulators. Toxicol Sci 69:79–91.

OECD. 1996. Organisation for Economic Co-operation and Development (OECD) Guidelines for the Testing of Chemicals, Section 4: Health Effects, Test No. 422: Combined Repeated Dose Toxicity Study with the Reproduction/Developmental Toxicity Screening Test. Adopted on 22 March, 1996.

OECD. 2009. Guidance Document for Histologic Evaluation of Endocrine and Reproductive Tests in Rodents Series on testing and assessment, number 106, OECD, Environmenta directorate, Joint meeting of the chemicals committee and the working party on chemicals, pesticides and iotechnology, Available at: http://www.oecd.org/officialdocuments/displaydocumentpdf/?cote=env/jm/mono(2009)11&doclanguage=en, accessed on July 28, 2011.

Ogle TF, Mills TM, Costoff A. 1990. Progesterone maintenance of the placental progesterone receptor and placental growth in ovariectomized rats. Biol Reprod 43:276–284.

Ohmori K, Kudo N, Katayama K, Kawashima Y. 2003. Comparison of the toxicokinetics between perfluorocarboxylic acids with different carbon chain length. Toxicology 184:135–140.

Olsen GW, Lange CC, Ellefson ME, Mair DC, Church TR, Goldberg CL, Herron RM, Medhdizadehkashi Z, Nobiletti JB, Rios JA, Reagen WK, Zobel LR. 2012. Temporal trends of perfluoroalkyl concentrations in American Red Cross Adult Blood Donors, 2000–2010. Environ Sci Technol 46:6330–6338.

Parker RM. 2006. Testing for reproductive toxicity. In: Hood RD, editor. Developmental and Reproductive Toxicology—A Practical Approach. Florida: CRC Press, Taylor & Fransis Group. pp 425–487.

Perkins RG, Butenhoff JL, Kennedy GL Jr, Palazzolo MJ. 2004. 13-week dietary toxicity study of ammonium perfluorooctanoate (APFO) in male rats. Drug Chem Toxicol 27: 361–378.

Permadi H, Lundgren B, Andersson K, Sundberg C, DePierre JW. 1993. Effects of perfluoro fatty acids on peroxisome proliferation and mitochondrial size in mouse liver: dose and time factors and effect of chain length. Xenobiotica 23:761–770.

Prevedouros K, Cousins IT, Buck RC, Korzeniowski SH. 2006. Sources, fate and transport of perfluorocarboxylates. Environ Sci Technol 40:32–44.

Rosol TJ, Yarrington JT, Latendresse J, Capen CC. 2001. Adrenal gland: structure, function, and mechanisms of toxicity. Toxicol Pathol 29:41–48.

Shallie PD, Fakoya FA, Fakunle PB, Haruna MT, Shotunde DF. 2012. Dietary stress and energy metabolism: Evaluation of the adrenal cortex. Webmed Central BIOCHEMISTRY 3: WMC003472.

Shi Z, Ding L, Zhang H, Feng Y, Xu M, Dai J. 2009a. Chronic exposure to perfluorododecanoic acid disrupts testicular steroidogenesis and the expression of related genes in male rats. Toxicol Lett 188:192–200.

Shi Z, Feng Y, Wang J, Zhang H, Ding L, Dai J. 2010a. Perfluorododecanoic acid-induced steroidogenic inhibition is associated with steroidogenic acute regulatory protein and reactive oxygen species in cAMP-stimulated Leydig cells. Toxicol Sci 114:285–294.

Shi Z, Zhang H, Ding L, Feng Y, Wang J, Dai J. 2010b. Proteomic analysis for testis of rats chronically exposed to perfluorododecanoic acid. Toxicol Lett 192:179–188.

Shi Z, Zhang H, Ding L, Feng Y, Xu M, Dai J. 2009b. The effect of perfluorododecanonic acid on endocrine status, sex hormones and expression of steroidogenic genes in pubertal female rats. Reprod Toxicol 27:352–359.

Shi Z, Zhang H, Liu Y, Xu M, Dai J. 2007. Alterations in gene expression and testosterone synthesis in the testes of male rats exposed to perfluorododecanoic acid. Toxicol Sci 98:206–215.

Tao L, Kannan K, Kajiwara N, Costa MM, Fillmann G, Takahashi S, Tanabe S. 2006. Perfluorooctanesulfonate and related fluorochemicals in albatrosses, elephant seals, penguins, and polar skuas from the Southern Ocean. Environ Sci Technol 40:7642–7648.

Thompson J, Roach A, Eaglesham G, Bartkow ME, Edge K, Mueller JF. 2011. Perfluorinated alkyl acids in water, sediment and wildlife from Sydney Harbour and surroundings. Mar Pollut Bull 62:2869–2875.

UK COT. 2006. COT statement on the tolerable risk daily intake for perfluorooctanoic acid, Committee on toxicity of chemicals on food, consumer products and the environment, October 2006.

US EPA. 2013. Perfluorooctanoic acid (PFOA) and fluorinated telomers, last updated on November 4, 2013. United States Environmental Protection Agency (US EPA). Available at: http://www.epa.gov/oppt/pfoa/. Accessed on February 28, 2014.

Van de Vijver KI, Holsbeek L, Das K, Blust R, Joiris C, De Coen W. 2007. Occurrence of perfluorooctane sulfonate and other perfluorinated alkylated substances in harbor porpoises from the Black Sea. Environ Sci Technol 41: 315–320.

Wang T, Lu Y, Chen C, Naile JE, Khim JS, Giesy JP. 2012. Perfluorinated compounds in a coastal industrial area of Tianjin, China. Environ Geochem Health 34:301–311.

Wolf CJ, Schmid JE, Lau C, Abbott BD. 2012. Activation of mouse and human peroxisome proliferator-activated receptor-alpha (PPARalpha) by perfluoroalkyl acids (PFAAs): Further investigation of C4-C12 compounds. Reprod Toxicol 33:546–551.

Yang Q, Xie Y, Alexson SE, Nelson BD, DePierre JW. 2002. Involvement of the peroxisome proliferator-activated receptor alpha in the immunomodulation caused by peroxisome proliferators in mice. Biochem Pharmacol 63:1893–1900.

Zhang H, Shi Z, Liu Y, Wei Y, Dai J. 2008. Lipid homeostasis and oxidative stress in the liver of male rats exposed to perfluorododecanoic acid. Toxicol Appl Pharmacol 227: 16–25.

Environmental Science & Technology

Article

pubs.acs.org/est

Isotope Microscopy Visualization of the Adsorption Profile of 2-Methylisoborneol and Geosmin in Powdered Activated Carbon

Yoshihiko Matsui,*[,†] Asuka Sakamoto,[‡] Soichi Nakao,[‡] Takuma Taniguchi,[‡] Taku Matsushita,[†] Nobutaka Shirasaki,[†] Naoya Sakamoto,[§] and Hisayoshi Yurimoto[§,∥]

[†]Faculty of Engineering, Hokkaido University, N13W8, Sapporo 060-8628, Japan

[‡]Graduate School of Engineering, Hokkaido University, N13W8, Sapporo 060-8628, Japan

[§]Isotope Imaging Laboratory, Creative Research Institution, Hokkaido University, N21W10, Sapporo, 001-0021, Japan

[∥]Natural History Sciences, Hokkaido University, N10W8, Sapporo 060-0810, Japan

Supporting Information

ABSTRACT: Decreasing the particle size of powdered activated carbon may enhance its equilibrium adsorption capacity for small molecules and micropollutants, such as 2-methylisoborneol (MIB) and geosmin, as well as for macromolecules and natural organic matter. Shell adsorption, in which adsorbates do not completely penetrate the adsorbent but instead preferentially adsorb near the outer surface of the adsorbent, may explain this enhancement in equilibrium adsorption capacity. Here, we used isotope microscopy and deuterium-doped MIB and geosmin to directly visualize the solid-phase adsorbate concentration profiles of MIB and geosmin in carbon particles. The deuterium/hydrogen ratio, which we used as an index of the solid-phase concentration of MIB and geosmin, was higher in the shell region than in the inner region of carbon particles. Solid-phase concentrations of MIB and geosmin obtained from the deuterium/hydrogen ratio roughly agreed with those predicted by shell adsorption model analyses of isotherm data. The direct visualization of the localization of micropollutant adsorbates in activated carbon particles provided direct evidence of shell adsorption.

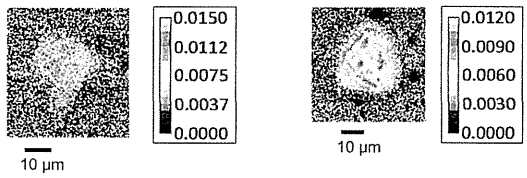

1. INTRODUCTION

Adsorption by powdered activated carbon (PAC) is a widely used method for removing micropollutants, in particular hydrophobic compounds, such as 2-methylisoborneol (MIB) and geosmin, earthly musty-smelling substances, in water treatment plants.[1,2] Although the MIB and geosmin adsorption capacities on PAC are high, the capacities are not fully utilized if the PAC−water contact times are insufficient, because adsorption kinetics are slow. To overcome the slow adsorption kinetics, superfine powdered activated carbon (SPAC) of particle diameter <1 μm is produced by microgrinding.[3] SPAC has also attracted attention, in particular for its potential use in combination with membrane microfiltration techniques.[4−7] In addition to SPAC having much faster adsorption kinetics than conventionally sized PAC, recent research has shown that SPAC has a greater equilibrium capacity to adsorb certain compounds such as large, chromophoric constituents of organic matter.[3,8] This increase in equilibrium adsorption capacity was not predicted because PAC and SPAC that was produced by microgrinding the PAC had a similar internal pore volume and a similar internal surface area. It has been traditionally thought that changing the particle size will not change its equilibrium adsorption capacity and the adsorption capacity of activated carbon does not depend on particle size because adsorption occurs in internal pores of activated carbon particles.[9]

In porous adsorbents, the increase in equilibrium adsorption capacity with decreasing particle size can be explained by shell adsorption, where adsorbates do not completely penetrate the adsorbent particle but instead preferentially adsorb near the outer surface of the particle (Supporting Information (SI) Figure S1).[10] Ando et al.[11] confirm the occurrence of shell adsorption for the adsorption of polystyrenesulfonate (molecular weight, 6000 Da) on carbon particles by directly observing intraparticle solid-phase concentration profiles of polystyrenesulfonate. As an index of polystyrenesulfonate concentration, they measured the emission of X-rays from sulfur atoms present in the polystyrenesulfonate by means of field emission−scanning electron microscopy/energy-dispersive X-ray spectrometry (FE-SEM/EDXS).

Our research group recently determined that the single-solute equilibrium capacity of activated carbon to adsorb MIB and geosmin, which are both small, nonchromophoric molecules, may be particle size−dependent. The occurrence of shell adsorption may accurately explain this phenomenon, but no direct evidence to support this hypothesis exists to date. Direct evidence is obtainable by observing the intraparticle concentration profile of MIB and geosmin. However, applicable

Received: May 20, 2014
Revised: August 25, 2014
Accepted: August 27, 2014
Published: August 27, 2014

Table 1. Characteristics of the Activated Carbons Examined[a]

	median diameter (D_{50}, μm)					
	conventionally sized PAC	superfine PAC	raw material	origin of conventionally sized PAC	isotherm	α (SAM parameter) $_{\mu m}-1$
carbon-A	31	2.6, 0.72, 0.50	coconut shell	SP23, Pica	MIB	0.24
					Geosmin	0.32
carbon-B	25	3.1, 0.85, 0.52	wood	MP23, Pica	MIB	0.03
					Geosmin	0.20
carbon-C	19	4.9, 0.62	wood	Taiko W, Futamura Chemical Co., Ltd.	MIB	0.09

[a]MIB, 2-methylisoborneol; PAC, powdered activated carbon; SAM, shell adsorption model.

methods have been limited. Very sophisticated methods such as measurements by means of atomic force microscopy can be applicable for the observation and determination of adsorption on flat model surfaces, but not for so well-defined and complicated surfaces such as activated carbon and cotton surfaces because of their shape, porous structure, and structural heterogeneity.[12−14] Fluorescence spectroscopy of the cotton surface that adsorbed fluorescently labeled polymer could determine the extent of adsorption,[15,16] but the method is not applicable for observing intraparticle concentration profile. Microprobe laser-desorption laser-ionization mass spectroscopy is used to spatially resolve intraparticle concentration profiles within several granular adsorbents,[17] but it is not be applicable to resolve profiles within adsorbents of particle diameter <30 μm. Direct observation with FE-SEM/EDXS has higher resolution but is not applicable for examining the adsorption of MIB and geosmin because these molecules do not contain a suitable marker atom since their constituent atoms are the same as those of activated carbon. These two methods give one-dimensional intraparticle concentration profile, but they cannot visualize concentration profile as a two-dimensional map.

Secondary ion mass spectrometry has been used to identify microscale isotope ratios in cosmic particles.[18] Isotope microscope systems, which are secondary ion mass spectrometers coupled with solid-state imaging detectors, enable microimaging of two-dimensional isotope ratios (e.g., deuterium/hydrogen ratio, $^2D/^1H$) with permil-level precision and high mass resolution.[19−21] Recently, isotope microscope systems have been used to analyze living matter and semiconductor specimens, in particular, isotope-doped samples.[22]

The objective of the present study was to visualize, for the first time, the intraparticle adsorption profile of trace organic compounds in PAC particles. The two taste and odor compounds, MIB and geosmin, were used as probe compounds in deuterium-labeled form. MIB and geosmin concentration profiles were visualized by using isotope microscopy to determine whether the phenomenon of the shell adsorption can explain the particle-size dependence of the equilibrium adsorption capacity of small, nonchromophoric adsorbates.

2. MATERIALS AND METHODS

2.1. Activated Carbons. Commercially available PACs of conventional particle size (median diameter >10 μm, Table 1) were obtained and prepared as slurries in ultrapure water (5% by weight). The PACs were pulverized into SPAC by wet grinding with a bead mill (Metawater Co., Tokyo, Japan). Median diameter SPAC particles ranged from 0.5 to 4.9 μm (Table 1, SI Figure S2). In the text, we refer to these activated carbons by using parenthetic numbers to indicate the particle median diameter in micrometers, for example, Carbon-A (31) represents the as-received form of Carbon-A. The activated carbons were stored as slurries in ultrapure water (Milli-Q Advantage, Millipore Co.) at 4 °C. Prior to use in experiments, slurries were diluted and placed under a vacuum prior to use.

Particle size distributions of the activated carbons were determined with a laser-light scattering particle size analyzer (Microtrac MT3300EXII; Nikkiso Co., Ltd., Tokyo, Japan) following the addition of a dispersant (Triton X-100; Kanto Chemical Co., Inc., Tokyo, Japan; final concentration after addition, 0.08%) and ultrasonic dispersion. Hydrogen contents in ~30-mg samples of each carbon were determined with an elemental analyzer (CHNS mode, 1150 °C in combustion tubes, 850 °C in reduction tube, vario EL cube, Elementar Analysensysteme GmbH, Germany). Prior to H analysis, carbons were dried for 12 house at a temperature of 105 °C and cooled in a desiccator.

2.2. Adsorbates and Water Samples. Stock solutions of MIB and geosmin were prepared by dissolving pure MIB or geosmin (Wako Pure Chemical Industries, Ltd., Osaka, Japan) in ultrapure water and then filtering the water through a 0.2 μm pore size membrane filter (DISMIC-25HP; Toyo Roshi Kaisha, Ltd., Tokyo). Organic-free water was prepared by amending ultrapure water with inorganic ions such that conductivity was 77−89 μS/cm and the ionic composition was similar to that used in a previous study.[3,23] However, natural organic matter, which largely affects the adsorption of MIB and geosmin on activated carbon, was not added. The organic-free water was spiked with the MIB or geosmin stock solutions to prepare samples with an initial MIB or geosmin concentration of ~1 μg/L, since MIB and geosmin occur naturally at concentrations usually lower than 1 μg/L. The water samples were adjusted to pH 7.0 ± 0.1 with HCl or NaOH as required. The concentrations of MIB and geosmin were confirmed by using a purge and trap concentrator (Aqua PT 5000 J; GL Sciences, Inc., Tokyo, Japan) coupled to a gas chromatograph−mass spectrometer (GCMS-QP2010 Plus; Shimadzu Corp., Kyoto, Japan).

2.3. Batch Adsorption Equilibrium Tests. Aliquots (150 mL) of the water samples containing MIB or geosmin (C_0 ~1 μg/L) were transferred to 160 mL vials. Specified amounts of SPAC or PAC were immediately added (0.05−1.0 mg/L) and the vials manually shaken and then agitated on a mechanical shaker for 1 week at a constant temperature of 20 °C. Preliminary experiments confirmed that the adsorption equilibrium for both MIB and geosmin was reached after 1 week of contact. Control tests were also conducted by using vials that did not contain carbon to confirm that changes in MIB and geosmin concentration during long-term mixing were negligible. After filtering the water samples through a 0.2 μm pore size membrane filter, MIB and geosmin concentrations in the aqueous phase were measured. Solid-phase concentrations

of MIB and geosmin were then calculated from the mass balance.

2.4. Isotope Microscopy. To prepare carbon particles loaded with deuterium-doped MIB or geosmin, we conducted batch adsorption experiments in 5 L bottles. Sample solutions containing approximately 1 μg/L deuterium-doped MIB or geosmin (Figure 1) were shaken after the addition of a specified

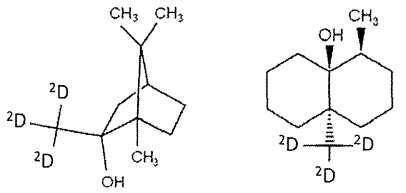

Figure 1. Chemical structures of deuterium-doped 2-methylisoborneol (left) and geosmin (right).

amount of carbon. After the bottles were shaken for 1 week, the carbon particles were recovered. Only the conventionally sized PACs were used for isotope microscopy because the intraparticle solid-phase concentration changed on a micrometer scale; therefore the solid-phase concentration would not measurably change in a SPAC particle. Another reason is that the image resolution of the isotope microscopy method is not sufficient to visualize MIB and geosmin concentration profiles in SPAC particles.

To prepare samples for imaging, the wet carbon particles were placed on an indium plate supported by a silicon wafer and partially embedded into the indium plate manually using gentle pressure. Further sample preparation, such as slicing with a microtome, was not conducted because activated carbon particles are very fragile and the inside of the particle was expected to be exposed during the isotope analysis.

Deuterium/hydrogen isotope analysis of the carbon particles was conducted by using an isotope microscope system (Hokkaido University, Sapporo, Japan) that consisted of a stigmatic secondary ion mass spectrometer (Cameca ims-1270) and a SCAPS (stacked complementary metal-oxide-semiconductor active pixel sensor) ion detector.[19] A 20 keV Cs^+ primary ion beam was homogeneously irradiated over a 250 × 250 μm^2 sample area to achieve uniform secondary ion-beam emission from an imaging area of 180 × 180 μm^2. The primary current was adjusted to 60 nA. We supposed that, during the exposure to the irradiation of the primary ion beam, shrinking of the carbon particles in size occurred, as depicted in Figure 2. In particular, the upsides of the carbon particles were removed and the insides of the particles were exposed. The secondary ions were accelerated to 10 keV and captured as mass-filtered ion images projected by the stigmatic ion optics of the secondary ion mass spectrometer. A 150 μm diameter focal plane aperture was used. The SCAPS ion detector was positioned on the projection plane of the mass-filtered secondary ion image. Secondary ion images of $^1H^+$ and $^2D^+$ were captured by the SCAPS ion detector with a repeated sequence of 5-s (^1H) and 250-s (^2D) detection times. Isotopic maps were obtained by calculating and plotting the $^2D/^1H$ molar ratio for each pixel. Loading of deuterium-doped MIB or geosmin in the carbon particles was expected to yield the $^2D/^1H$ ratio much higher than that of the earth's natural $^2D/^1H$ molar ratio of 0.00015.[24]

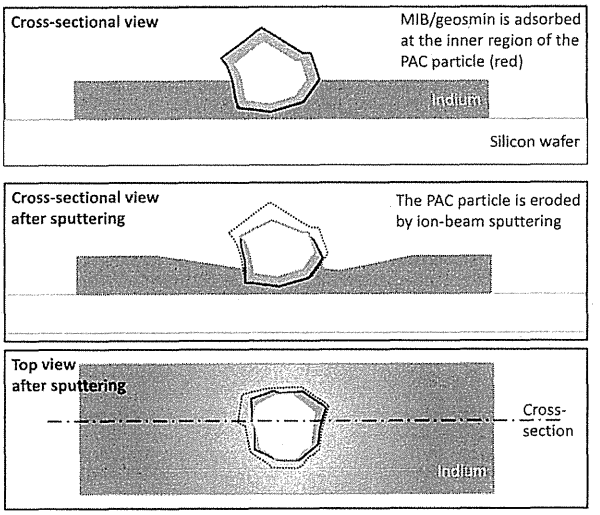

Figure 2. Schematic of the change in particle size caused by ion-beam sputtering in the repeated detection of secondary ions. MIB: 2-methylisoborneol; PAC, powdered activated carbon.

3. RESULTS AND DISCUSSION

3.1. Effect of Particle Size on MIB and Geosmin Adsorption Capacity. The adsorption of MIB on Carbon-A was particle-size dependent (i.e., the equilibrium adsorption capacity was greater for the SPACs than for the PAC). To be precise, the adsorption capacity increased when the particle diameter was decreased from 31 to 2.6 μm, but it did not change when the particle diameter was reduced further, to 0.72 or 0.50 μm. On the other hand, results for Carbon-B and Carbon-C showed only a small particle-size dependency for the entire particle size range tested (25–0.52 μm, Figure 3 and SI Table S1). The adsorption of geosmin on both tested carbons tested (Carbon-A and Carbon-B) was also particle-size dependent, with greater equilibrium adsorption capacity for SPAC than for PAC.

We previously reported that for NOM adsorption, the particle-size dependency of the equilibrium adsorption capacity was not due to the pore size distributions of SPAC and PAC. In this study, we confirmed that the pore size distributions in both mesopore and micropore regions did not change substantially as a result of the pulverization of PAC for the production of SPAC (SI Table S1 and Figure S3). Similarly, changes in BET surface area were small. Therefore, the particle-size dependency of MIB and geosmin adsorption capacities was not related to the pore sizes of the PACs and the SPACs. The particle size dependency was greater for Carbon-A than for Carbon-B and Carbon-C. However, the difference in particle size dependency was also not related to the pore size distributions of the carbons (SI Table S1 and Figure S2). Further research is needed to reach any conclusive remarks regarding the manner in which these characteristics influence the dependency of adsorption capacity on particle size.

Overall, the dependency of the adsorption capacity on particle size was greater for geosmin than for MIB, and geosmin was adsorbed to a greater extent than MIB in both the SPAC and PAC. The effect of adsorbate characteristics on the particle size dependency of the adsorption capacity requires further study. The dependency decreases with the order geosmin > MIB > phenol,[3] where no measurable dependency was

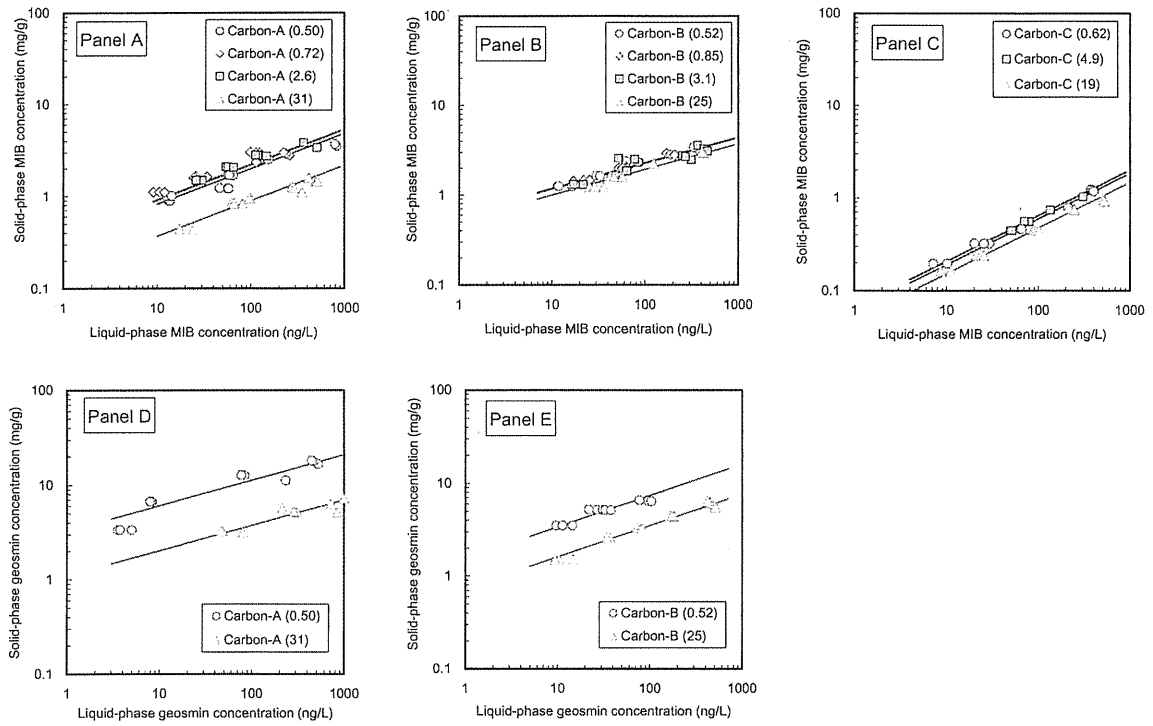

Figure 3. Adsorption isotherms of 2-methylisoborneol (MIB; panels A–C) and geosmin (panels D–E). Lines represent fits for the shell adsorption model.

observed for the latter adsorbate.[3] It is possible that the hydrophobicity of the adsorbate plays a role, whose greater particle size dependency is associated with increasing adsorbate hydrophobicity.

3.2. Prediction of the Solid-Phase Concentration Profiles. For NOM adsorption, Ando et al.[3] report that the increase in adsorption capacity with decreasing adsorbent particle size is attributable to molecules adsorbing principally in the exterior region close to the external particle surface. The specific external surface area (surface area per unit mass) available for adsorption is greater for smaller adsorbent particles, and hence adsorption capacity is larger on SPAC. The shell adsorption model (SAM) was proposed to describe quantitatively the increase in NOM adsorption capacity with decreasing carbon particle size.[10] In this study, the SAM was applied for MIB and geosmin, and solid-phase concentration profiles in carbon particles were predicted. The SAM utilizes an expanded expression of the Freundlich equation.

$$q_E = KC_E^{1/n} \tag{1}$$

where q_E is the equilibrium solid-phase concentration of the adsorbate (mg/g), C_E is the equilibrium aqueous-phase concentration (ng/L), K is the Freundlich adsorption capacity parameter $(mg/g)/(ng/L)^{1/n}$, and n is the Freundlich exponent.

In the SAM, the adsorption capacity is locally different in a adsorbent particle, and the local adsorption capacity parameter, that is, the Freundlich K_S value, decreases linearly with distance from the external surface to a certain depth. When assuming a spherical adsorbent particle:

$$K_S(r, R) = K_0 \times \max[(r - R) \times \alpha + 1, 0] \tag{2}$$

where $K_S(r, R)$ is the radially changing local Freundlich adsorption capacity parameter $(mg/g)/(ng/L)^{1/n}$, r is the radial distance from the center of a adsorbent particle (μm), R is the adsorbent particle radius (μm), K_0 is the Freundlich parameter of adsorption at the external particle surface (i.e., at $r = R$, $[mg/g]/[ng/L]^{1/n}$) and α is the reciprocal of penetration depth (or thickness of the penetration shell) with the unit μm^{-1}.

Therefore, the local solid-phase concentration, $q(r,R)$, at radial distance r in an adsorbent with radius R is given by substituting eq 2 into Freundlich equation.

$$q(r, R) = C_E^{1/n}K_0 \times \max[(r - R) \times \alpha + 1, 0] \tag{3}$$

where $q(r,R)$ is the radially changing local solid-phase concentration as a function of radial distance r and carbon particle radius R $(mg/g)/(ng/L)^{1/n}$.

When the adsorbent particle size is not uniform, the overall adsorption capacity is given by

$$q_E = \int_0^\infty \{\int_0^R r^2 q(r, R)dr\}\frac{3f_R(R)}{R^3}dR \tag{4}$$

where $f_R(R)$ is the normalized particle size distribution function of adsorbent (μm^{-1}).

After substituting eq 3 into 4, the isotherm equation of the SAM becomes

$$q_E = C_E^{1/n}K_0 \int_0^\infty \{\int_0^R r^2 \max[(r - R) \times \alpha + 1, 0]dr\} \frac{3f_R(R)}{R^3}dR \tag{5}$$

To fit eq 5 to the isotherm data shown in Figure 3, we searched for sets of isotherm parameter values for K_0, α, and n

dx.doi.org/10.1021/es5024515 | Environ. Sci. Technol. 2014, 48, 10897–10903

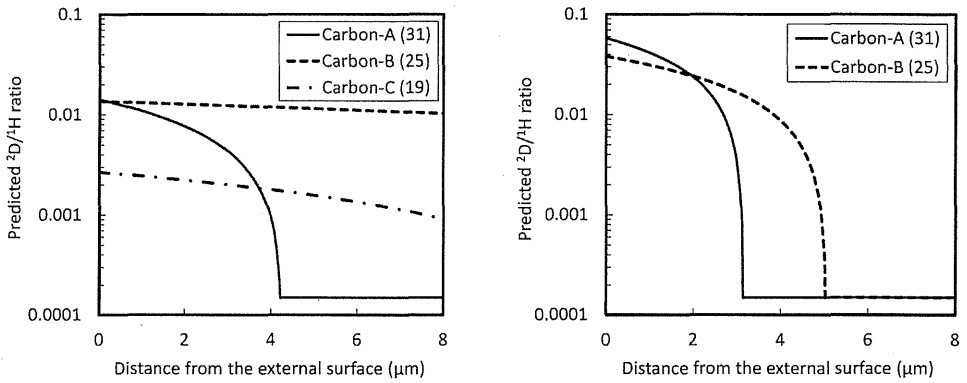

Figure 4. Deuterium/hydrogen ratios against distance from the external surface of a carbon particle predicted by using the shell adsorption model (left, MIB; right, geosmin). Calculations were made for an equilibrium aqueous-phase concentration of 100 ng/L.

that best fit each MIB and geosmin adsorption isotherm of Carbon-A, Carbon-B, and Carbon-C. The SAM successfully described the effect of adsorbent particle size on MIB and geosmin adsorption capacities. Equation 2 of the SMA implies (1) when the adsorbent particle is large enough compared to the penetration depth, the interior region of the adsorbent particle is not used, and adsorption capacity increases with decreasing adsorbent particle size and (2) when the adsorbent particle is small enough compared to the penetration depth, the entire interior region of the adsorbent particle as well as the external region can be utilized for adsorption, and the adsorption capacity is independent of adsorbent particle size. For the case of the MIB adsorption on Carbon-A, the penetration depth ($1/\alpha$) of the SMA was ~4 μm (Table 1). Therefore, the adsorption capacity of increased when the particle diameter was decreased from 31 to 2.6 μm, but it did not change when the particle size was reduced further, to 0.72 or 0.50 μm (Figure 3). For the case of the MIB adsorption on Carbon-B, the penetration depth was ~30 μm, which was larger than the particle diameter of Carbon-B (Table 1). Therefore, the adsorption capacity did not change in the particle size range from 25 to 0.52 μm. The penetration depth differed markedly among carbons, which made adsorption capacity dependency/independency on carbon particle size.

By using eq 3 with the searched parameter values, we next predicted solid-phase concentration profiles across the radius of a carbon particle for deuterium-doped MIB and geosmin adsorbates, in which three hydrogen atoms were replaced with three deuterium atoms (Figure 1). Using the hydrogen content of the carbon particles as determined by the elemental analysis (SI Table S2) and assuming that the earth's natural deuterium/hydrogen molar ratio is 0.00015,[24] we predicted the solid-phase concentration profile of the deuterium/hydrogen ratio along the radius of as-received carbon particles for MIB and geosmin adsorptions (Figure 4). The deuterium/hydrogen atomic ratios decreased from the external surface to the inner region, but for MIB adsorption on Carbon-B and Carbon-C the decrease was less dramatic than for Carbon-A, for which a penetration distance of only ~4 μm was predicted. The deuterium/hydrogen ratio of the outer shell region (to a depth of ~3 μm) of a Carbon-A (31) particle was predicted to be between 0.004 and 0.013 (Figure 4, left), and these values are >30 times those for the inner region (>4 μm penetration depth). For the adsorption of geosmin, a higher deuterium/hydrogen ratio was predicted for the outer surface region than for MIB, and the penetration distances for geosmin were shorter than for MIB for both Carbon-A and Carbon-B (Figure 4, right).

3.3. Direct Observation of the Solid-Phase Concentration Profile by Means of Isotope Microscopy. The solid-phase concentration profile was directly observed by using deuterium-doped MIB and Carbon-A (31), which is an adsorbent in which adsorption capacity is particle size-dependent. Prior to visualizing the solid-phase concentration profile, we confirmed that deuterium-doped MIB had the same adsorbability as the nondoped MIB used in the isotherm experiments (Figure 5).

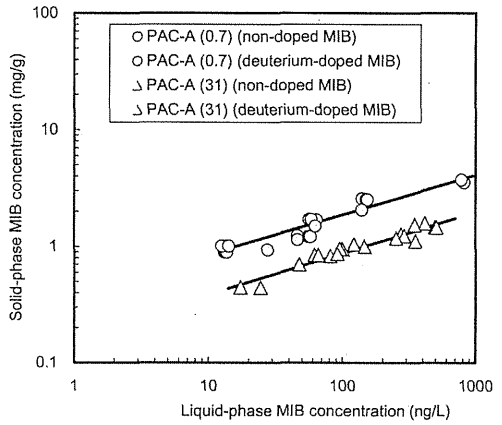

Figure 5. Adsorption isotherms of deuterium-doped 2-methylisoborneol (MIB) and nondoped MIB. PAC, conventionally sized powdered activated carbon.

A series of secondary ^2D and ^1H images of a Carbon-A (31) particle loaded with deuterium-doped MIB was taken (SI Figure S4A). Isotopographs were obtained by calculating the ratio of ^2D detection ($^2D\_2$ in SI Figure S4A) to ^1H detection (average of $^1H\_1$ and $^1H\_2$ in SI Figure S4A) for each pixel of the image, as shown in Figure 6A. The $^2D/^1H$ ratio was higher than that of the earth's natural $^2D/^1H$ molar ratio of 0.00015, indicating the presence of deuterium-doped MIB that was loaded on the carbon particle. The $^2D/^1H$ ratios across the particle qualitatively confirm greater loading of MIB (higher $^2D/^1H$ ratio) on the exterior region close to the outer-surface of the particle. The trend was confirmed by measurements of another Carbon-A (31) particle also loaded with deuterium-

dx.doi.org/10.1021/es5024515 | Environ. Sci. Technol. 2014, 48, 10897−10903

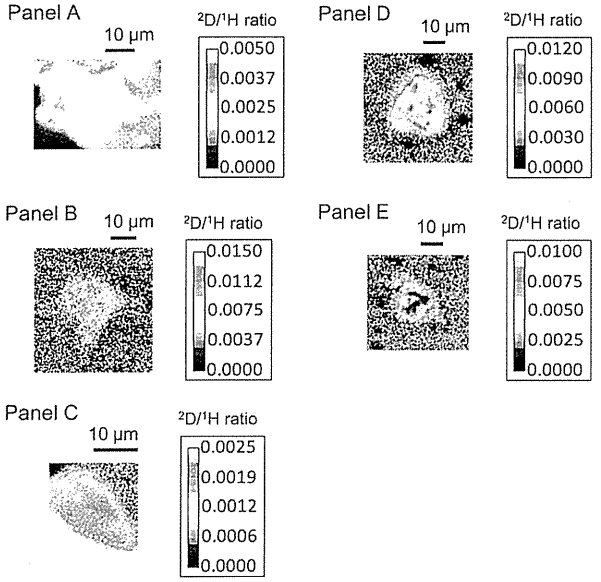

Figure 6. Isotopic maps (deuterium/hydrogen ratio) of carbon particles loaded with deuterium-doped 2-methylisoborneol (MIB) or geosmin. Panel A: coconut-based Carbon-A (31) loaded with deuterium-doped MIB. Panel B: wood-based Carbon-B (25) loaded with deuterium-doped MIB. Panel C: wood-based Carbon-C (19) loaded with deuterium-doped MIB. Panel D: coconut-based Carbon-A (31) loaded with deuterium-doped geosmin. Panel E: wood-based Carbon-B (25) loaded with deuterium-doped geosmin. White dotted lines indicate periphery estimated from the ^{1}H images.

doped MIB (SI Figure S5A). The shell adsorption model predicted a ^{2}D/^{1}H ratio at the exterior region of 0.004 to 0.013; observed ratio was somewhat lower at around 0.004 but roughly agreed with the prediction. The center region exhibits ^{2}D/^{1}H ratios that are ~2−3 times lower than those in the exterior region. It should be noted that the center region of the image (Figure 6A) does not correspond to a radial position of r = 0 as only a portion of the PAC particle was ablated by ion sputtering as shown in Figure 2.

We next examined Carbon-B (25) and Carbon-C (19), which are adsorbents in which adsorption capacity is particle size-independent. For these carbons, we expected MIB to be adsorbed on internal pore surfaces as well as in the external region. For Carbon-B (25), the ^{2}D/^{1}H ratios were locally high in the internal region, but overall uniform across the particle (Figure 6B, a series of secondary ^{2}D and ^{1}H images are shown in SI Figure S4B), thereby verifying that MIB adsorbs on interior pore surfaces of Carbon-B (25). For Carbon-C (19), detections were repeated 10 times and during detection a reduction in particle size was clearly observed (SI Figure S4C). We attribute this reduction in size to ablation by ion-beam sputtering, which removed some parts of the particle, in particular the upper part, resulting in a gradual reduction in particle size. Uniform ^{2}D/^{1}H ratios across the particle were observed, in particular after the third ^{2}D detection, suggesting that the inside of the particle was exposed by the ion beam sputtering after the third ^{2}D detection. Furthermore, the observed ^{2}D/^{1}H ratios of Carbon-B (25) and Carbon-C (19) (Figure 6B, C) were consistent with the ^{2}D/^{1}H ratio predicted by the shell adsorption model (Figure 4, left). These observations confirm that MIB adsorbs internally on Carbon-B (25) and Carbon-C (19).

We similarly examined the adsorption of deuterium-doped geosmin on Carbon-A (31) and Carbon-B (25). According to the shell adsorption model analysis, geosmin molecules were predicted to adsorb mainly on the exterior region of particles of Carbon-A (31) and Carbon-B (25); therefore, a high ^{2}D/^{1}H ratio at the exterior region was expected (Figure 4, right). A greater loading of geosmin (high ^{2}D/^{1}H ratio) near the outer surface of the particles was clearly observed for both Carbon-A (31) and Carbon-B (25) (Figure 6D, E; a series of ^{2}D and ^{1}H images are shown in SI Figure 3D, E). Clearer pictures were recorded for the geosmin experiments compared with the MIB experiments, which could possibly be due to the greater loading of geosmin compared with that of MIB (see Figure 3).

In this research, isotopic maps of the deuterium/hydrogen ratio, which was a marker of the solid-phase concentration of deuterium-doped MIB and geosmin molecules, provided the direct evidence of the location of adsorbed MIB and geosmin molecules on activated carbon particles. In PAC that had smaller equilibrium adsorption capacity than SPAC, MIB and geosmin principally adsorbed in the exterior shell region of the PAC particles. In contrast, in PAC that had a similar equilibrium adsorption capacity to SPAC, MIB adsorbed more evenly throughout entire PAC particles. Together these results confirm the validity of the shell adsorption theory in which molecules do not completely penetrate the adsorbent particle but instead preferentially adsorb near the outer surface of the particle. The observed equilibrium higher adsorption capacity on SPAC than on PAC was therefore due to the larger external surface area on which the molecules preferentially adsorb.

However, all experiments were conducted in NOM-free waters, but not in natural waters where NOM competition is a significant factor on adsorption.[25] Traditionally, competition is discussed in terms of pore blockage and direct site competition where NOM and micropollutant adsorb in the same pore.[26,27] Our research revealed that micropollutants may adsorb in the external region of carbon particles, that is, in the same region in which chromophoric NOM preferentially adsorbs. Therefore, our results imply that competition is severer when both NOM and micropollutant adsorb in the external region.

■ ASSOCIATED CONTENT

Supporting Information

Tables S1 and S2 and Figures S1 to S4 are available. This material is available free of charge via the Internet at http://pubs.acs.org.

■ AUTHOR INFORMATION

Corresponding Author

*Phone/fax: +81-11-706-7280; e-mail: matsui@eng.hokudai.ac.jp.

Notes

The authors declare no competing financial interest.

■ ACKNOWLEDGMENTS

This study was supported by grants-in-aid for Scientific Research S (24226012) and Challenging Exploratory Research (25550049) from the Japan Society for the Promotion of Science and by a Health and Labour Sciences Research Grant (Research on Health Security Control).

REFERENCES

(1) Chowdhury, Z. K.; Summers, R. S.; Westerhoff, G. P.; Leto, B. J.; Nowack, K. O.; Corwin, C. J. *Activated Carbon: Solutions for Improving Water Quality*; American Water Works Association: Denver, CO, 2012.

(2) Srinivasan, R.; Sorial, G. A. Treatment of taste and odor causing compounds 2-methyl isoborneol and geosmin in drinking water: A critical review. *J. Environ. Sci.* **2011**, *23* (1), 1–13.

(3) Ando, N.; Matsui, Y.; Kurotobi, R.; Nakano, Y.; Matsushita, T.; Ohno, K. Comparison of natural organic matter adsorption capacities of super-powdered activated carbon and powdered activated Carbon. *Water Res.* **2010**, *44* (14), 4127–4136.

(4) Ellerie, J. R.; Apul, O. G.; Karanfil, T.; Ladner, D. A. Comparing graphene, carbon nanotubes, and superfine powdered activated carbon as adsorptive coating materials for microfiltration membranes. *J. Hazard. Mater.* **2013**, *261* (0), 91–98.

(5) Cai, Z.; Wee, C.; Benjamin, M. M. Fouling mechanisms in low-pressure membrane filtration in the presence of an adsorbent cake layer. *J. Membr. Sci.* **2013**, *433* (0), 32–38.

(6) Huang, H.; Schwab, K.; Jacangelo, J. G. Pretreatment for low pressure membranes in water treatment: A review. *Environ. Sci. Technol.* **2009**, *43* (9), 3011–3019.

(7) Heijman, S. G. J.; Hamad, J. Z.; Kennedy, M. D.; Schippers, J.; Amy, G. Submicron powdered activated carbon used as a pre-coat in ceramic micro-filtration. *Desalin. Water Treat.* **2009**, *9* (1–3), 86–91.

(8) Dunn, S. E.; Knappe, D. R. U. *DBP Precursor and Micropollutant Removal by Powdered Activated Carbon*; Water Research Foundation: Denver, CO, 2013.

(9) Sontheimer, H.; Crittenden, J. C.; Summers, R. S. *Activated Carbon for Water Treatment*. DVGW-Forschungsstelle, Engler-Bunte-Institut; Universitat Karlsruhe (TH), 1988.

(10) Matsui, Y.; Ando, N.; Yoshida, T.; Kurotobi, R.; Matsushita, T.; Ohno, K. Modeling high adsorption capacity and kinetics of organic macromolecules on super-powdered activated carbon. *Water Res.* **2011**, *45* (4), 1720–1728.

(11) Ando, N.; Matsui, Y.; Matsushita, T.; Ohno, K. Direct observation of solid-phase adsorbate concentration profile in powdered activated carbon particle to elucidate mechanism of high adsorption capacity on super-powdered activated carbon. *Water Res.* **2011**, *45* (2), 761–767.

(12) Zimin, D.; Craig, V. S. J.; Kunz, W. Adsorption and desorption of polymer/surfactant mixtures at solid–liquid interfaces: Substitution experiments. *Langmuir* **2004**, *20* (19), 8114–8123.

(13) Zimin, D.; Craig, V. S. J.; Kunz, W. Adsorption pattern of mixtures of trimethylammonium-modified hydroxyethylcellulose and sodium dodecyl sulfate at solid–liquid interfaces. *Langmuir* **2004**, *20* (6), 2282–2291.

(14) Trabelsi, S.; Langevin, D. Co-adsorption of carboxymethyl-cellulose and cationic surfactants at the air–water interface. *Langmuir* **2006**, *23* (3), 1248–1252.

(15) Hoffmann, I.; Oppel, C.; Gernert, U.; Barreleiro, P.; von Rybinski, W.; Gradzielski, M. Adsorption isotherms of cellulose-based polymers onto cotton fibers determined by means of a direct method of fluorescence spectroscopy. *Langmuir* **2012**, *28* (20), 7695–7703.

(16) Hoffmann, I.; Theile, M.; Grätz, S.; Scholz, J.; Barreleiro, P.; von Rybinski, W.; Gradzielski, M. On the influence of surfactants on the adsorption of polysaccharide-based polymers on cotton studied by means of fluorescence spectroscopy. *Langmuir* **2012**, *28* (31), 11400–11409.

(17) Ahn, S.; Werner, D.; Karapanagioti, H. K.; McGlothlin, D. R.; Zare, R. N.; Luthy, R. G. Phenanthrene and pyrene sorption and intraparticle diffusion in polyoxymethylene, coke, and activated carbon. *Environ. Sci. Technol.* **2005**, *39* (17), 6516–6526.

(18) Sakamoto, N.; Seto, Y.; Itoh, S.; Kuramoto, K.; Fujino, K.; Nagashima, K.; Krot, A. N.; Yurimoto, H. Remnants of the early solar system water enriched in heavy oxygen isotopes. *Science* **2007**, *317* (5835), 231–233.

(19) Yurimoto, H.; Nagashima, K.; Kunihiro, T. High precision isotope micro-imaging of materials. *Appl. Surf. Sci.* **2003**, *203–204* (0), 793–797.

(20) Benninghoven, A.; Rüdenauer, F. G.; Werner, H. W. *Secondary Ion Mass Spectrometry: Basic Concepts, Instrumental Aspects, Applications and Trends*; Wiley: New York, 1987.

(21) Kita, N. T.; Ushikubo, T.; Fu, B.; Valley, J. W. High precision SIMS oxygen isotope analysis and the effect of sample topography. *Chem. Geol.* **2009**, *264* (1–4), 43–57.

(22) Hamasaki, T.; Matsumoto, T.; Sakamoto, N.; Shimahara, A.; Kato, S.; Yoshitake, A.; Utsunomiya, A.; Yurimoto, H.; Gabazza, E. C.; Ohgi, T. Synthesis of 18O-labeled RNA for application to kinetic studies and imaging. *Nucleic Acids Res.* **2013**, DOI: 10.1093/nar/gkt344.

(23) Matsui, Y.; Yoshida, T.; Nakao, S.; Knappe, D. R. U.; Matsushita, T. Characteristics of competitive adsorption between 2-methylisoborneol and natural organic matter on superfine and conventionally sized powdered activated carbons. *Water Res.* **2012**, *46* (15), 4741–4749.

(24) Drever, J. I. *The Geochemistry of Natural Waters: Surface and Groundwater Environments*; Prentice Hall PTR, 1997.

(25) Chen, G.; Dussert, B. W.; Suffet, I. H. Evaluation of granular activated carbons for removal of methylisoborneol to below odor threshold concentration in drinking water. *Water Res.* **1997**, *31* (5), 1155–1163.

(26) Guo, Y.; Yadav, A.; Karanfil, T. Approaches to mitigate the impact of dissolved organic matter on the adsorption of synthetic organic contaminants by porous carbonaceous sorbents. *Environ. Sci. Technol.* **2007**, *41* (22), 7888–7894.

(27) Summers, R. S.; Knappe, D. R. U.; Snoeyink, V. L. Adsorption of organic compounds by activated carbon. In *Water Quality and Treatment: A Handbook of Community Water Supplies*; Edzwald, J. K.; American Water Works Association, McGraw-Hill, 2011; Chapter 14.

The Journal of Toxicological Sciences (J. Toxicol. Sci.)
Vol.39, No.1, 97-108, 2014

Original Article

Repeated dose and reproductive/developmental toxicity of perfluoroundecanoic acid in rats

Mika Takahashi[1], Shigeru Ishida[2], Mutsuko Hirata-Koizumi[1], Atsushi Ono[1] and Akihiko Hirose[1]

[1]*Division of Risk Assessment, Biological Safety Research Center, National Institute of Health Sciences, 1-18-1 Kamiyoga, Setagaya-ku, Tokyo 158-8501, Japan*
[2]*Gotemba Laboratory, Bozo Research Center Inc., 1284 Kamado, Gotemba-shi, Shizuoka 412-0039, Japan*

(Received September 6, 2013; Accepted November 30, 2013)

ABSTRACT — Perfluoroalkyl acids (PFAAs) are environmental contaminants that have received attention because of their possible effects on wildlife and human health. In order to obtain initial risk information on the toxicity of perfluoroundecanoic acid (PFUA), we conducted a combined repeated dose toxicity study with the reproduction/developmental toxicity screening test (OECD test guideline 422). PFUA was administered by gavage to rats at 0 (vehicle: corn oil), 0.1, 0.3 or 1.0 mg/kg/day. At 1.0 mg/kg/day, body weight gain was inhibited in both sexes, and there was a decrease in fibrinogen in both sexes and shortening of the activated partial thromboplastin time in males. An increase in blood urea nitrogen and a decrease in total protein in both sexes and increases in alkaline phosphatase and alanine transaminase and a decrease in albumin in males were observed at 1.0 mg/kg/day. Liver weight was increased in males at 0.3 mg/kg/day and above and in females at 1.0 mg/kg/day, and this change was observed after a recovery period. In both sexes, centrilobular hypertrophy of hepatocytes was observed at 0.3 mg/kg/day and above and focal necrosis was observed at 1.0 mg/kg/day. In reproductive/developmental toxicity, body weight of pups at birth was lowered and body weight gain at 4 days after birth was inhibited at 1.0 mg/kg/day, while no dose-related changes were found in the other parameters. Based on these findings, the no observed adverse effect levels (NOAELs) for the repeated dose and reproductive/developmental toxicity were considered to be 0.1 mg/kg/day and 0.3 mg/kg/day, respectively.

Key words: Perfluoroundecanoic acid, Repeated dose toxicity, Reproductive and developmental toxicity, Screening test, Rat

INTRODUCTION

Perfluoroalkyl acids (PFAAs) are environmental contaminants that have received attention because of their possible effects on wildlife and human health in recent years; PFAAs are very stable in the environment, have bioaccumulation potential, and have been detected in environmental media and biota in many parts of the world, including oceans and the Arctic; and many researchers have revealed their toxic effects, including hepatotoxicity and reproductive/developmental toxicity in laboratory animals, as reviewed by ATSDR (2009) and Hirata-Koizumi *et al.* (2012). In particular, perfluorooctane sulfonate (PFOS) and perfluorooctanoic acid (PFOA) are the most effective surfactants among PFAAs (Lau *et al.*, 2007), and many toxicological effects of PFOS and PFOA have been revealed (reviewed in ATSDR, 2009, and fully introduced in Hirata-Koizumi *et al.*, 2012). PFOS and PFOA have now been regulated worldwide, and the manufacture, import and use of PFOS were essentially prohibited in the EU in 2008 (DIRECTIVE 2006/122/EC) and in Japan in 2010 (Japanese law, 2009). As with PFOS, there is growing momentum to strengthen the regulation of PFOA.

Perfluoroundecanoic acid (PFUA, C11) is one of the higher homologue chemicals of PFOA, and PFUA is used as an alternative to PFOA, which is used as a processing aid in the manufacture of fluoropolymers (EPA, 2013a). Although the annual production and import volume of PFUA was not available, that of perfluoroalkyl carboxylic acids (PFCAs, C2-C10) in Japan was reported to be 1,000

Correspondence: Akihiko Hirose (E-mail: hirose@nihs.go.jp)

to 10,000 tons in 2007 and less than 1,000 tons in 2010 (CHRIP, 2013). The production and import volume of PFUA is considered to have fallen in recent years globally (EPA, 2013b). However, it is necessary to be concerned about the toxicological potential of PFUA even though its production and import volume has been reduced, due to its very persistent and highly bioaccumulative characteristics (ECHA, 2012). Moreover, long-chain (C9-C20) PFCAs can be detected in the environment as degradates from commercial fluorotelomers (Environment Canada, 2010). In humans, total exposure to PFUA is not available, but the mean concentration of PFUA in human serum collected in the U.S. was < 1 ng/ml (Calafat *et al.*, 2006, 2007a and 2007b; Kuklenyik *et al.*, 2004), and the maximum concentration in breast milk was 0.056 ng/ml (So *et al.*, 2006), as summarized by ATSDR (2009). In Sweden, estimated dietary exposure to PFUA increased (88, 158 and 212 pg/kg/day in 1999, 2005 and 2010, respectively) along with an increase in the quantified concentration of PFUA in fish products (Vestergren *et al.*, 2012). Domingo *et al.* (2012) summarized that the major dietary source of the estimated intake of PFUA was fish and shellfish.

In order to obtain initial risk information on the toxicity of PFCAs, which have a longer chain than PFOA (C8), we have carried out a series of screening tests on the toxicity of PFCAs (C11-C18), and the result for perfluorooctadecanoic acid (PFOdA, C18) has been already published (Hirata-Koizumi *et al.*, 2012). Here, we show initial risk information on the repeated dose and reproductive/developmental toxicity of PFUA (C11).

MATERIALS AND METHODS

This study was performed in compliance with OECD guideline 422 "Combined Repeated Dose Toxicity Study with the Reproduction/Developmental Toxicity Screening Test," and in accordance with the principles for Good Laboratory Practice (MOE *et al.*, 2003, 2008) at the BOZO Research Center (Shizuoka, Japan). The experiment was performed in accordance with the Japanese regulations on animal welfare (Japanese law, 2005).

Animals and housing conditions

Crl:CD(SD) rats (8 weeks old) were purchased from Atsugi Breeding Center (Charles River Laboratories Japan, Inc., Kanagawa, Japan). This strain was chosen because it is most commonly used in toxicity studies, including reproductive and developmental toxicity studies, and historical control data are available. The animals were acclimatized to the laboratory for 15 days and subjected to treatment at 10 weeks of age. They were carefully observed during the acclimation period, and male and female rats found to be in good health were selected for use. In addition, vaginal smears of each female were recorded, and only females showing a normal estrous cycle were used in the experiment. One day before the initial treatment, the rats were distributed into four main groups of 12 males and 12 females, and two additional satellite groups (control and highest dose groups) of five females, each by stratified random sampling based on body weight. For males, 5/12 animals each in the main groups of control and highest dose were used as the satellite groups.

Throughout the study, animals were maintained in an air-conditioned room set at 20-27°C, with relative humidity set at 31-69%, a 12-hr light/dark cycle, and ventilation with > 10 air changes/hr. A basal diet (NMF; Oriental Yeast Co., Ltd., Tokyo, Japan) and tap water were provided *ad libitum*. The rats were housed individually, except for mating and nursing periods. From day 17 of pregnancy to the day of sacrifice, individual dams and/or litters were reared using wood chips as bedding (White Flake; Charles River Laboratories Japan, Inc.).

Chemicals and dosing

PFUA (CAS RN: 2058-94-8) was obtained from Wako Chemical, Ltd. (Miyazaki, Japan), stored in a light-blocking bottle and kept at room temperature. The PFUA (Lot no. TSM0481) used in this study was 98.5% pure, and stability during the study was verified by gas chromatography. The test article was suspended in corn oil (Wako Pure Chemical Industries, Ltd., Osaka, Japan), and administered to the animals by gastric intubation. Control rats received the vehicle alone. Dosing solutions were prepared at least once per eight days, stored under refrigeration until dosing, and dosed at room temperature, as stability under these conditions has been confirmed. The concentrations of PFUA in the formulations were within the acceptable range (97.0-101.8%).

The dose levels were chosen based on the results of a 14-day dose range-finding study conducted at levels of 2, 6, 20, 60, 200, and 600 mg/kg/day. In this range-finding study, deaths were observed in 5/5 males and 4/5 females at 20 mg/kg/day, and in all animals at 60 mg/kg/day or more, and an increase in liver weight in both sexes and increases in ALP and BUN in males were observed at 2 and 6 mg/kg/day. PFAAs including PFUA are persistent and bioaccumulative (ATSDR, 2009). Taking into account that the length of the dosing period in the present study was about three times than that in the dose range-finding study, the highest dose in the present study was set at 1.0 mg/kg/day. Finally, the dose levels of PFUA in

the present study were set as 0.1, 0.3 or 1.0 mg/kg/day.

Twelve males per group were dosed for 42 days, beginning 14 days before mating. After the administration period, 5 of 12 males per group were reared for the recovery period of 14 days without administration of PFUA, as satellite groups. The main group females were dosed for 41-46 days, beginning 14 days before mating to day 4 of lactation throughout the mating and gestation period. Females in the satellite group were given PFUA for 42 days, followed by the recovery period of 14 days. The first day of dosing was designated as day 0 of administration and the day after the final dose was designated as day 0 of the recovery period. The volume of each dose was adjusted to 5 ml/kg body weight based on the latest body weight.

Observations

All rats were observed daily for clinical signs of toxicity. Body weight was recorded twice a week in all males and in the satellite group females, and twice a week during the premating period, on days 0, 4, 7, 11, 14, 17, and 20 of pregnancy and on days 0 and 4 of lactation in main group females. Food consumption was recorded twice a week in all males and in satellite group females, and twice a week during the premating period, on days 1, 4, 7, 11, 14, 17, and 20 of pregnancy and on days 2 and 4 of lactation in main group females. Functional observation battery (FOB) in all animals was recorded once a week during the administration period, as follows: (i) home cage observation; posture, convulsion, and abnormal behavior, (ii) in-the-hand observation; ease of removal from cage and handling, fur and skin condition, eye ball, secretion from nose and/or eye, visible mucous membrane, lacrimation, salivation, piloerection, pupil diameter, and respiration, and (iii) open field observation; arousal, ambulation, posture, shivering, convulsion, rearing frequency, excreta, stereotypical behavior, and abnormal behavior.

Five animals in each group were subjected to the following observations and examinations unless noted otherwise. Sensory reactions for pupillary reflex, approximation reflex, tactile reflex, auditory reflex, pain reflex, righting reflex and width of the landing legs, grip strength of fore and hind limbs, and spontaneous motor activity were tested in main group males on day 37 of administration, in main group females on day 4 of lactation, and in satellite group males and females on day 37 of administration and on day 8 of the recovery period. Fresh urine was sampled from animals using a urine-collecting cage during the last weeks of the dosing and recovery periods. The 4-hr urine samples were collected soon after dosing under fasting (water was allowed *ad libitum*), and the 20-hr urine samples were collected, food and water being allowed *ad libitum*.

After 16-20 hr (overnight) of fasting, the main group of rats was euthanized by exsanguination under anesthesia on the day after the final administration in males and on day 4 of lactation in females, and satellite group rats were euthanized on the day of the completion of the recovery period. The external surfaces of the rats were examined. The abdomen and thoracic cavity were opened, and gross internal examination was performed. Blood samples were drawn from the abdominal aorta. Major organs were removed from all animals, and the brain, thyroid, thymus, heart, liver, spleen, kidney, adrenal glands, testis, epididymis were weighed. The numbers of corpora lutea and implantation sites were counted in all main group females. The testes and epididymides were fixed with Bouin's solution and in 10% phosphate-buffered formalin. Other organs were stored in 10% phosphate-buffered formalin. The cerebrum and cerebellum, pituitary gland, spinal cord, sciatic nerve, thyroid, parathyroid, adrenal glands, thymus, spleen, mandibular lymph nodes, mesenteric lymph node, heart, lung, trachea, stomach, duodenum, jejunum, ileum, cecum, colon, rectum, liver, kidney, bladder, testis, epididymis, uterus, seminal vesicle, sternum, and femur were histopathologically evaluated for five males and females in the control and the highest groups, and organs with macroscopically abnormal findings were also examined histopathologically. The organs for histopathological evaluations were processed routinely for embedding in paraffin, and sections were prepared for staining with hematoxylin–eosin. Test substance-related histopathological changes were found in the liver in males and females, and in the stomach in males; therefore, the liver in all animals and the stomach in all males were also examined histopathologically.

The 4-hr urine samples were tested for color, pH, protein, glucose, ketone body, bilirubin, occult blood, urobilinogen, and urinary sediment. Urinary sediment was stained and examined microscopically. The 20-hr urine samples were tested for osmotic pressure. Urine volume for 4-hr and 20-hr was measured. In the collected blood samples the red blood cell (RBC) count, hemoglobin, platelet count, and white blood cell count were measured. In addition, mean corpuscular volume (MCV), hematocrit, mean corpuscular hemoglobin (MCH), mean corpuscular hemoglobin concentration (MCHC), reticulocyte rate, and differential leukocyte rates were calculated. Prothrombin time (PT), activated partial thromboplastin time (APTT), and fibrinogen were determined. Blood chemistry was tested for alkaline phosphatase (ALP), total protein, albumin, albumin/globulin (A/G) ratio, total bilirubin, blood